5-2024

Modelling Terrestrial and Potential Extraterrestrial Photopigments via Density Functional Theory

Dorothea Illner
Florida Institute of Technology, dillner2022@my.fit.edu

Modelling Terrestrial and Potential Extraterrestrial Photopigments via Density Functional Theory

By Dorothea Illner

A thesis submitted to the College of Science and Engineering of
Florida Institute of Technology
in partial fulfillment of the requirements
for the degree of

Master of Science
in
Chemistry

Melbourne, Florida
May, 2024

We the undersigned committee hereby approve the attached thesis,
"Modelling Terrestrial and Potential Extraterrestrial Photopigments via Density Functional Theory."
by
Dorothea Illner

_____

Roberto Peverati, Ph.D.
Associate Professor
Chemistry and Chemical Engineering
Major Advisor

_____

Manasvi Lingam, Ph.D.
Assistant Professor
Aerospace, Physics, and Space Sciences

_____

Boris Akhremitchev, Ph.D.
Associate Professor
Chemistry and Chemical Engineering

_____

Jessica Smeltz, Ph.D.
Associate Professor and Interim Department Head
Chemistry and Chemical Engineering

Abstract

Title: Modelling Terrestrial and Potential Extraterrestrial Photopigments via Density Functional Theory

Author: Dorothea Illner

Advisor: Roberto Peverati, Ph.D.

In the search for extraterrestrial life, biosignatures play a crucial role in identifying its putative traces. A commonly known and robust biosignature is the Vegetation Red Edge (VRE), which can be described as a sharp increase of reflectance observed from a planet and stems from the light absorption of photopigments in specific regions in the electromagnetic spectrum. For Earth, this VRE is known to occur around 700 nm, however, if the photopigments absorb light in different regions and have different structures the VRE could experience a wavelength shift.

In this work, Chlorophyll a and a potential photopigment precursor called Phot0 were computationally modeled using a variety of DFT functionals. The results indicate that these photopigments are best described using the PW6B95 global hybrid functional or the B2PLYP double hybrid functional since both of these methods provide relatively accurate results at low computational cost. Additionally, the influence of the metal center on the peak shift in the absorption spectrum of phot0 was explored. Elements with a higher electronegativity than magnesium, which is the metal center found in chlorophylls, shift the peak towards a lower wavelength, while a relatively lower electronegativity of the metal center results in a redshifted peak.

Table of Contents

List of Figures

List of Tables

List of Abbreviations

ATP	Adenosine Triphosphate
BChl	Bacteriochlorophyll
B3LYP	Becke, 3-parameter, Lee-Yang-Parr
CAM	Coulomb-Attenuating Method
CCSD	Coupled Cluster Theory with Single and Double Excitations
Chl	Chlorophyll
CIS	Configuration Interaction Singles
CT	Charge Transfer
DFA	Density Functional Approximation
DFT	Density Functional Theory
DH	Double Hybrid
DLPNO	Domain-based Localpair Natural Orbital Implementation
EA	Electron Affinity
EET	Excitation Energy Transfer
EOM	Equation Of Motion
ET	Electron Transfer
eV	Electron Volt
GGA	Generalized Gradient Approximation
GH	Global Hybrid
GS	Ghost States
HD	Hybrid Density
HF	Hartree-Fock
HOMO	Highest Occupied Molecular Orbital
I	Ionization energy
IP	Ionization Potential
KS	Kohn-Sham
LDA	Local Density Approximation
LUMO	Lowest Unoccupied Molecular Orbital
MGGA	Meta- Generalized Gradient Approximation
MUE	Mean Unassigned Error
RSH	Range Separated Hybrid
PBE	Perdew-Burke-Ernzerhof
PNO	Pair Natural Orbital
RC	Reaction Center
RPA	Random Phase Approximation
STEOM	Similarity Transformed Equation of Motion
TDDFT	Time-Dependent Density Functional Theory
TDM	Transition Dipole Moment
UEG	Uniform Electron Gas

UV/ Vis	Ultra Violet/ Visible
VEE	Vertical Excitation Energy
VRE	Vegetation Red Edge
WFT	Wave Function Theory
XC	Exchange-correlation
ZPE	Zero Point Energy

Acknowledgement

I would like to thank Dr. Peverati and Dr. Lingam for the chance to work on interesting research projects, like this one.

Dr. Peverati, you taught me so much about computational chemistry and helped me get started in this field. Thanks to you, I worked hands-on with a variety of programs and gained a tremendous amount of knowledge about theoretical concepts.

Moreover, I would like to thank Dr. Lingam for the encouragement and guidance provided. Your lectures opened up my eyes for new topics and possibilities.

I am also thankful to Dr. Akhremitchev for the inspiring talks and support throughout my time at Florida Tech.

Lastly, I am extremely grateful to my family and friends for their encouragement, patience, and never-ending support.

Dedication

This thesis is dedicated to my family, who made it possible for me to come to the USA and study at this great institution. I want to specially thank my mom, grandmother, and grandfather for always lending an open ear and being so invested in my life, even though we are so far apart. Moreover, I want to thank my friends and mentors for their invaluable advice and inspiration. Lastly, am thankful for my boyfriend for being understanding, patient and always believing in me. This thesis is dedicated to all those who have believed in me and stood by my side every step of the way.

Chapter 1
Photosynthesis

1.1 Photosynthesis

Photosynthesis can be described as a metabolic pathway that produces chemical energy utilizing light energy. The synthesis of organic compounds from inorganic materials happens in the presence of sunlight, which explains the name photosynthesis in which "photo" originates from the Greek word *phōs* meaning light.[1] The term photosynthesis is commonly used to describe oxygenic photosynthesis where carbon dioxide and water produce carbohydrates and oxygen as a byproduct. In the light reaction carbon dioxide is captured from the air, bound in the plants, and then used to produce organics (e.g. carbohydrates). The general reaction of photosynthesis is shown below, potential carbohydrate products are for example glucose $C_6H_{12}O_6$.[2]

$$CO_2 + H_2O \xrightarrow{h\nu} CH_2O + O_2 \quad (1)$$

Photosynthesis is well known to be one of the most important bioprocesses on Earth. The importance of photosynthesis is shown in the fact that about 80% of all the biomass on Earth consists of photosynthetic organisms.[3] To get a better understanding of the order-of-magnitude photosynthesis has, one might want to look into the paper by Field *et al*., published in 1998.[4] They explore the net primary production (NPP), which has been defined as the amount of carbon that is fixated in the photosynthetic process and is available to "*the first heterotrophic level in an ecosystem*".[5] Field *et al*. explain that a global NPP of around 104.9 petagrams carbon is reached per year. Obviously, these numbers are partly outdated, but show the significance of photosynthesis on Earth. A more modern example is provided by Frankelius *et al*. in their paper from 2020 where they explained that cereals alone were responsible for the capture of 3,825 Tg of carbon dioxide every year.[6]

1.1.1 Transformation of light energy into electrochemical free energy

Generally, photosynthesis involves two main processes; the light-dependent and light-independent (dark) reaction. Light-dependent reactions are initiated as soon as the photopigment absorbs a photon which causes it to lose an electron. This thesis focuses on the light-dependent reaction and explores how photopigments capture light in the following paragraphs.

Photopigments play an important role in photosynthesis since they are able to harvest light. The most well-known example of photopigments are chlorophylls (Chls). In 1932 Emerson and Arnold revolutionized the understanding of functional pigment organization with their experiment that revealed

that it takes 2500 chorophylls and relatively high light intensities to produce one oxygen molecule in 10 minutes.[7] They illuminated a cell suspension of green alga *Chlorella* with repetitive 10 µs flashes and observed that only a small fraction amongst all chlorophylls is directly involved in the transformation of electronically excited states into the primary electrochemical product.[8] These new results helped Gaffron and Wohl to develop the idea of photosynthetic units that organize pigments and functionally distinguish them into two main groups. About 99% of all pigments are involved in light absorption and aid in the transfer of the electronically excited states to the place of the photochemical reaction.[8]

The majority of pigments, symbolized by P_A, form a light-harvesting device called an antenna. This assists in the enhancement of the optical cross-section of photochemically active pigments, here referred to as P_{RC} with RC symbolizing reaction centers. In figure 1 the basic mechanism for antenna pigments P_A and reaction center pigments P_{RC} is visualized in the framework of a HOMO/LUMO scheme, with HOMO and LUMO referring to the highest occupied and lowest unoccupied molecular orbitals. The two pigment molecules (P_1 and P_2) with matching orbital structures exhibit a so-called electronic coupling and symbolize either antenna or RC pigments. In the beginning, P_1 is in the first excited electronic singlet state (here represented with $^1P_1$*), while P_2 starts in the electronic ground state. From here two different electronic interactions can occur between $^1P_1$* and P_2. Either a radiation less excitation energy transfer (EET) happens, or an electron transfer (ET) takes place. An ET demonstrates how RC pigments behave, while the EET reflects the basic principle of antenna pigments. In an EET an exciton is transferred to another pigment molecule, shown in the figure below with green arrows.[8] The term "exciton" was originally used in solid-state physics to define electronically excited states in crystals.[9]

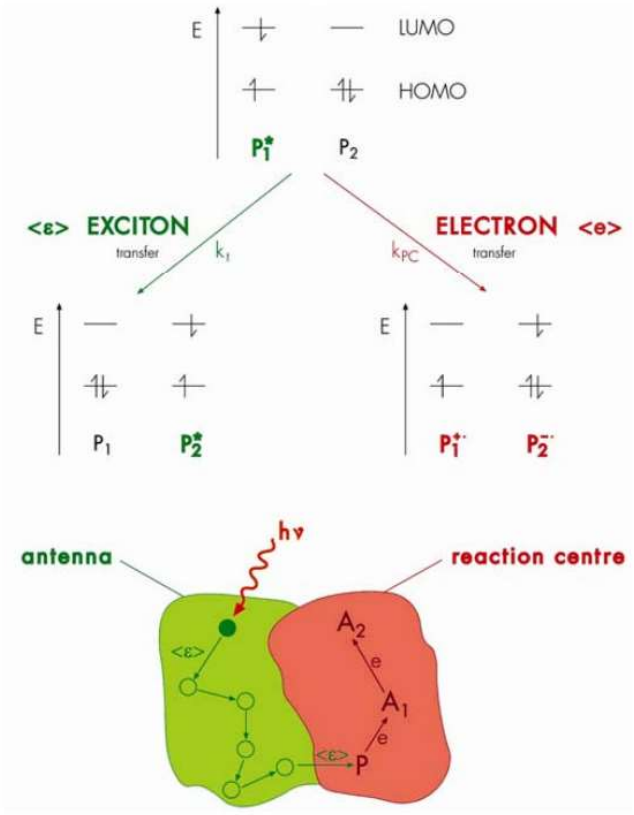

Figure 1: Visualization of the basic mechanism for the functions of P_A and P_{RC}. P_1 and P_2 represent two pigment molecules with matching orbital structures. ($^1P_1$* is the first excited electronic singlet state of the P_1 molecule, while P_1 and P_2 are the electronic ground states). HOMO and LUMO refer to the highest occupied and lowest unoccupied molecular orbitals. The diagram illustrates the excitation energy transfer (EET, green) and electron transfer (ET, red) processes. In the lower portion, an antenna (green) and reaction center (red) complex is shown, with ⟨ε⟩ and ⟨e⟩ representing exciton and an electron, and k_t and k_{PC} representing the rate constants for EET and ET. Lastly, A_1/A_2 are electron acceptor components.[8]

On the other hand, an ET leads to the formation of ion radical pairs $P_1^{+\bullet}$ $P_2^{-\bullet}$ where the excited pigment transfers an electron to the ground state P_2. Here $^1P_1$* and P_2 are coupled and P_2 serves as an electron acceptor. ET represents the function of a photochemically active pigment P_{RC}, while EET reflects the underlying principle of P_A.[8]

As established earlier photosynthesis is one of the most important biochemical pathways due to its direct or indirect occurrence in nearly all life on Earth.[10,11] This complex process occurs in plants, but also algae and bacteria. Some bacteria perform anoxygenic photosynthesis utilizing bacteriochlorophyll to split hydrogen sulfide. Hydrogen sulfide is the equivalent of water in this case yielding sulfur instead of oxygen as a byproduct. Another form of phototrophy occurring in prokaryotes (bacteria and archaea) is a type of non-carbon-fixing anoxygenic pathway.[12] As rightly noted by the author, "*Rhodopsins do not mediate electron transfer reactions—they can perform phototrophy but not photosynthesis*".[12]

In this case, photopigment retinal and microbial rhodopsin derivates absorb light in the green region to synthesize adenosine triphosphate directly via proton pumps. This version of phototrophy appears to be ancient, and may have existed in the Paleoarchean. Moreover, it constitutes a sizable fraction of all oceanic phototrophy documented on modern Earth.[13]

On the whole, many scientists think that the first organisms important for photosynthesis were reducing agents like hydrogen or hydrogen sulfide which evolved early in Earth's history.[14,15] Afterwards cyanobacteria evolved contributing directly to the oxygenation of Earth by producing an excess of oxygen; making the path for the evolution of complex life.[13]

1.2 Extraterrestrial Photosynthesis

Photosynthesis on earth works due to the absorption of light, emitted by our sun. The sun emits light within a broad wavelength spectrum, of which humans can see only a small range, called the visible spectrum from approximately 400 to 750 nm, while the majority of electromagnetic radiation stays hidden.[16] Green plants contain different photopigments, like chlorophylls (Chls), which absorb light at a different wavelength. Chlorophyll a (Chl a) is the primary photopigment for oxygenic photosynthesis in many organisms, including plants, algae, or cyanobacteria.[17] Many photopigments, such as Chl a, absorb light at a peak wavelength of 680 and 700 nm.[8,13,14] However, the sun emits the strongest spectral energy flux at around 550 nm, while the highest photon flux occurs around 650 nm.[15]

There is no guarantee that photosynthesis on extraterrestrial planets uses photopigments similar to those found on earth. Other star systems provide different conditions, which makes it likely that photosynthesis and photopigments are adjusted to such. Lehmer *et al*. published a paper in 2021 and described how different stars emit light with different peak absorbance wavelengths.[18] They describe that in other star systems, various chlorophyll derivates are likely to be formed. Lehmer *et al*. used Björns method, which was optimized by Marosvölgyi and van Gorkom to compute the absorption-based photon flux.[18,19]

Aside from Lehmer, many other scientists explore the possibilities of photosynthesis on earth-like planets (ELPs).[20–26] Wolstenscroft and Raven discuss conditions on Earth that led to O_2-producing photosynthesis on Earth and theorize how photosynthesis can evolve on ELPs, considering various factors (liquid water, UV radiation). The paper moreover explores to what extend parent star type and geological processes influence the O_2 generation and photosynthetic productivity.[20]

Another work by Kiang *et al.* focuses on biosignatures from ELPs orbiting different star types. They simulate a variety of atmospheric compositions and conclude that photopigments show a different absorption peak wavelength depending on the star system they are in.[21]

Very recently Duffy *et al.* published a paper discussing photosynthesis on ELPs orbiting closely around ultracool red dwarf stars. These systems are interesting, because the photosynthetically active region in the emission spectrum is very limited, meaning that oxygenic photosynthesis might be unable to occur and anoxygenic photosynthesis is in the focus. The paper contains an assessment of properties needed for optimal antenna absorption at a certain spectral flux and predicts absorption spectra of potential photopigments.[22]

Lingam *et al*. published a variety of work on this topic. They developed a quantum-mechanic model, to aid in the exploration of excitation features of photopigments, by assuming that the host star´s spectral photon flux determines the absorption maximum of photopigments.[23] On the other hand, they published two papers concerning prospective life on ELPs around brown dwarfs.[24,25] The first paper discusses the total habitable volume of brown dwarfs, which can be defined as a range of conditions for the presence of liquid water. This habitable volume, which was explored for effective temperatures ranging from 250 to 300 K, is claimed to be approximately 2 orders of magnitude higher than that of ELPs. Moreover, the importance of photosynthesis and other factors is studied for the facilitation of life.[25] In the other paper they specifically focus on three factors: 1) The expected life time of planets in the habitable zone, 2) The photon fluxes needed for oxygenic photosynthesis, 3) ultraviolet (UV) radiation fluxes necessary for prebiotic reactions (origin of life).[24]

Lastly, Lingam and Loeb explore the possibility of photosynthesis occurring on rocky planets with a permanent nightside, driven by light reflected from exomoons. Additionally, prospective photosynthesis is analyzed for habitable exomoons with light reflected from the planet they are orbiting. The results indicate that this planet-moon system can be feasible, if the star mass $M_\star$ is bigger or approximately 0.2 the planet mass $M_\odot$ ($M_\star \gtrsim 0.2 M_\odot$).[26]

1.3 Extraterrestrial photosynthesis and biosignatures

A common strategy that scientists follow in the search for extraterrestrial life is to extrapolate from our Earth, a planet with life. Therefore, one could imagine the existence of photosynthesis on other worlds, which leads to the question of detecting such. Scientists search for so-called “biosignatures”, which are commonly defined as substances, objects, and/ or patterns that originate from biological agents.[27] Des Marais et al. provide a better idea of biosignatures in their compendium written in 2008.[28] Their list includes, for example, atmospheric gases, temporal changes, cellular and extracellular morphologies, as well as bio-organic molecular structures.[15] Schwieterman et al. provide a more recent overview of biosignatures.[29]

There are two common biosignatures of photosynthesis which can be considered canonical. The term canonical refers to biosignatures that are unique to life and not produced abiotically.[30] The first important signature to look out for is molecular oxygen O_2.

Molecular oxygen is produced as a side product in photosynthesis and is hypothetically detectable by spectroscopes. The O_2-A band occurs around 760 nm while the O_2-B band is found at approximately 690 nm.[29] O_2 is the best-studied remote-sensing biosignature that is known to have several false positives and moreover serves as the classic example of false negatives.[31,32] A false negative describes the suppression of the generated biosignature, which prevents their detection.[33] A robust biosignature is a signature that indicates the existence of life and has no known false positives (or negatives).[34] A robust interpretation of biosignatures includes their environmental factors. Since oxygen is so well studied, its framework helps assess potential biosignature candidates.[35] Earth's history shows how oxygen rise is dependent on the planet's evolution of oxygenic photosynthesis and geochemical dynamics favorable for the long-term accumulation of significant amounts of oxygen.[36,37]

The second important biosignature that we focus on in this work is called Vegetation Red Edge (VRE). It is defined as a spectral biosignature describing a region in the electromagnetic spectrum where the reflectance changes rapidly. Most chlorophylls show a decline in absorbance beyond the Q_y band around 650-700 nm. In comparison to O_2, the VRE is a robust biosignature. Moreover, photopigments are like chlorophylls canonically perceived as possible reliable indicators of extraterrestrial life.[38]

1.4 Photopigments

As mentioned earlier photopigments are molecules that can participate in photosynthesis by light-harvesting. Since the process of photosynthesis varies from species to species, it is to be expected that different photopigments evolved. This thesis is supported by the fact that all photosynthesis mechanisms start when light energy is absorbed by so-called reaction centers, which are proteins that contain photosynthetic pigments or chromophores.

Chlorophylls are found in almost all organisms that undergo photosynthesis, like plants, algae, and bacteria. Plants and algae commonly contain chlorophyll a and b, but algae additionally use other photopigments, like carotenoids (shown in figure 2). The majority of algae and plants contain Chl a to collect light used for photosynthesis. Green algae and euglenophytes moreover use Chl b, while other algae use many different combinations of chlorophylls, carotenoids, or phycobiliproteins to collect light with different wavelengths.[39] Bacteria commonly contain Chl a, phycobiliproteins, bacteriochlorophylls, or carotenoids. In cyanobacteria Chl a and phycobiliproteins were found, purple bacteria comprise BChl a and Bchl b, and research proved that green sulfur bacteria contain Bchl e and Bchl c.[39] Thus, a variety

of pigments (both chlorophylls and otherwise) are documented in photosynthetic organisms on Earth, though our focus will be exclusively on the former.

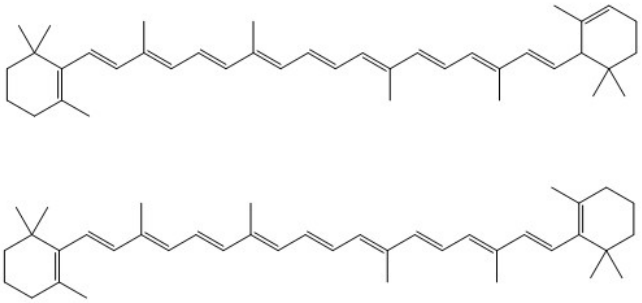

Figure 2: Molecular structure of Carotenoid a (upper structure) and b (lower structure).

1.4.1 Chlorophylls

Chlorophylls form one of the most important and well-known classes of photopigments responsible for photosynthesis.[39] The name leads back to the Greek words *khloros* translation meaning "pale green" and *phyllon* meaning "leaf".[1] Generally, chlorophylls have three major roles in photosynthesis: 1) Absorbance of light in the light-harvesting complexes or antennas, 2) Transfer of excitation energy with a high quantum efficiency to the reaction centers, 3) Charge separation across the photosynthetic membrane, which generates reducing agents (electron donors) and ATP over a simultaneously generated membrane potential.[39]

There are nearly 100 different chlorophyll structures known, for example, the most well-known chlorophyll a and chlorophyll b[39]. The different structures for chlorophyll a and b are shown below and illustrate the porphyrin ring structure chlorophylls contain, as well as their magnesium center ion (figure 3). As one can tell from the structures shown in figure 3, chlorophylls break the D_{4h} symmetry. This has a crucial influence on the orbital energies and breaks the degeneracy for the idealized D_{4h} molecule.[40]

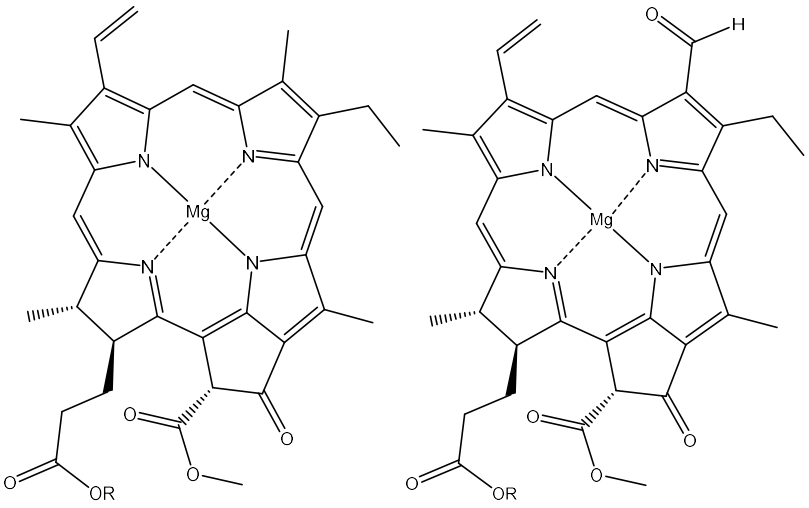

Figure 3: Structures for Chlorophyll a (Chl a) shown on the left, and for Chlorophyll b (Chl b) on the right, with R representing the side chain $C_{20}H_{39}$, were built using ChemDraw20.0.

The spectroscopic properties of chlorophylls can be described using the Gouterman model, which involves the excitation between four different frontier orbitals: HOMO-1, HOMO, LUMO, and lastly LUMO+1.[41] If one assumes an idealized D_{4h} symmetry on the molecules, the two occupied orbitals experience a transformation to two degenerate orbitals called a_{2u} and a_{1u}. On the other hand, the two unoccupied orbitals transform into a set of degenerate e_g orbitals. For transitions between these orbitals, one expects two excited states with ^1E_u character, which are split in their energy by orbital mixing. As a result, two absorption bands are expected to occur in absorption spectra. Firstly, the B-band also referred to as the Soret band, is expected at a lower wavelength with relatively high intensity, and secondly, the Q-band at a higher wavelength, but with relatively low intensity.[40] The B-band is found around 380 to 420 nm, while the weaker Q band is observed between 500 to 800 nm.[42] However, this model is inaccurate for ideal D_{4h} symmetry because the HOMO-1 and HOMO and the LUMO and LUMO+1 are degenerate, meaning that only one signal will be seen in the absorption spectrum since the transitions share the same excitation energy due to the degeneracy of the orbitals.

To label the transitions one can use the polarization direction implemented into the macrocycle plane and with its origin set at the Mg^{2+} ion. The x-axis is oriented along the NH···NH coordinate of the porphyrin, which is furthermore indicated in Figure 4 below. The Q_y transition is expected to have the lowest energy, as indicated in Figure 4. The other transitions are expected to show increasing energy in the following order: Q_x, to B_x, and lastly to B_y. Accordingly, y-labeled transitions should mainly correspond to the transitions from HOMO→ LUMO and HOMO-1 → LUMO+1, while x-labeled transitions refer to HOMO-1 → LUMO as well as HOMO → LUMO+1 transition.

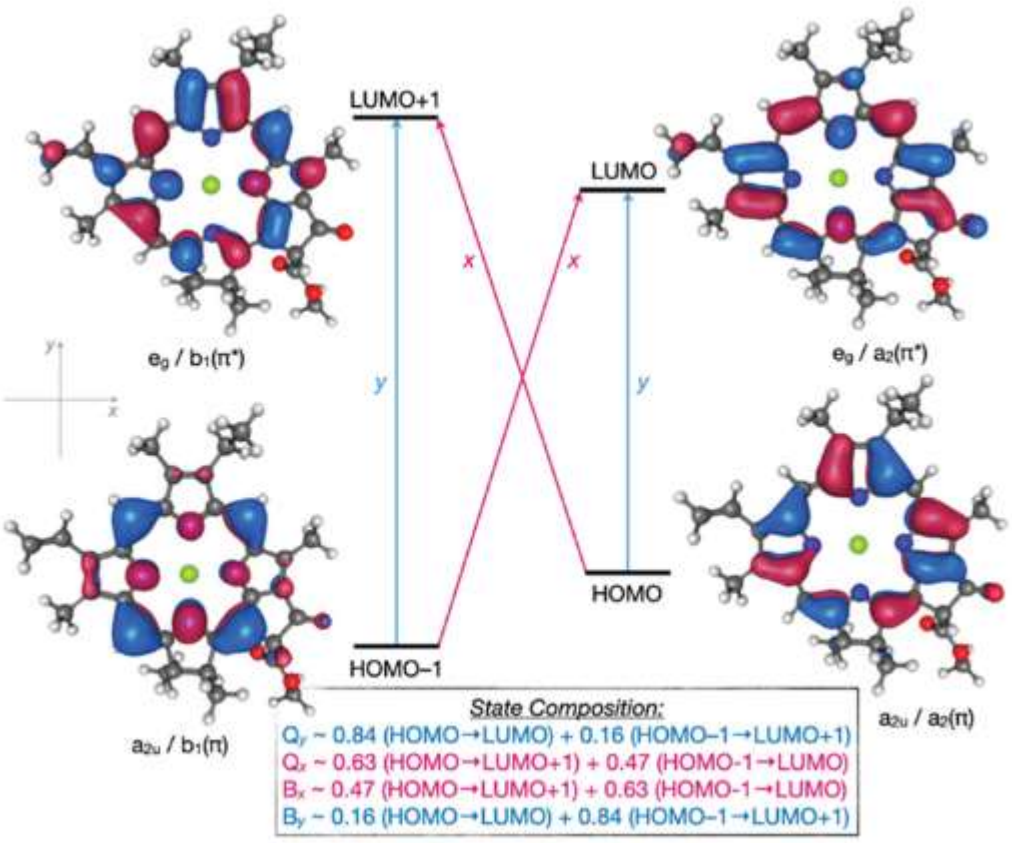

Figure 4: Frontier Molecular Orbitals (MOs) calculated for Chl a using CAM-B3LYP-D3(BJ) and the def2-TZVP basis set. The labeling of the orbitals was done in two different ways: first using the porphyrin ring geometry (D_{4h} point group; labels are shown in the figure to the left of "/") and chlorin (C_{2v} point group; labels are shown in the figure to the right of "/"). Every one-electron Gouterman transition and the associated dipole moment shows either an x-polarization (Q_x and B_x; pink arrows) or a y-polarization (B_y and Q_y; blue arrows). In the inset are the approximated state compositions of the four transitions reported, which were calculated with CAM-B3LYP-D3(BJ)/def2-TZVP.[40]

Obtaining experimental gas-phase spectra of chlorophylls is quite challenging since neutral Chls decompose easily. For that reason chlorophyll spectra were historically obtained in solution, however, computational models are mainly focused on the accurate calculation of low-lying excited states of Chls.[43–49] However, solvent effects can cause interferences, which were generally neglected, prohibiting such calculations from being used as a benchmark.[50,51] Figure 5 shows an example of the absorption spectra of various photopigments calculated in monodisperse solutions.

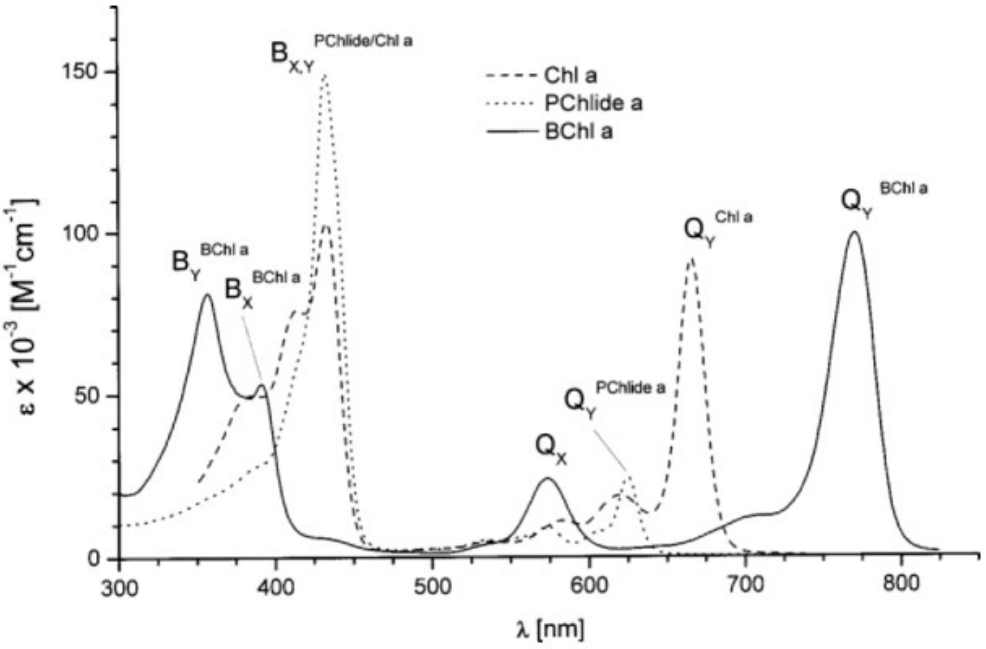

Figure 5: Absorption spectra of Chl a and PChlide a and BChl a calculated in monodisperse solutions with absorption band assignment based on the four-orbital model.[39]

Recently, however, accurate gas-phase spectra of charged Chls were produced by tagging molecules with cations and measuring with action spectroscopy.[42,52–54] Sirohiwal *et al*. used the experimental data obtained by Gruber *et al*. by tagging Chl a with tetramethylammonium (figure 6) and combined it with calculations utilizing the domain-based local pair natural orbital implementation of the similarity transformed equation of motion coupled cluster theory with single and double excitations (DLPNO-STEOM-CCSD, explained in section 2.1.9) to report energy shifts and correct the experimental absorption maxima to vertical excitation energies (VEEs, explained in section 1.5).[42,55] Therefore, Sirohiwal *et al*. report quasi-experimental VEEs for Chl a in their paper, which allows for the comparison of calculated VVEs directly to gas-phase spectra.[56] They moreover, calculated and analyzed the band shape by using two different approaches that use an optimized geometry of the ground state and assume that the excited state can be approximated by a Hessian optimization step that is single augmented.[55]

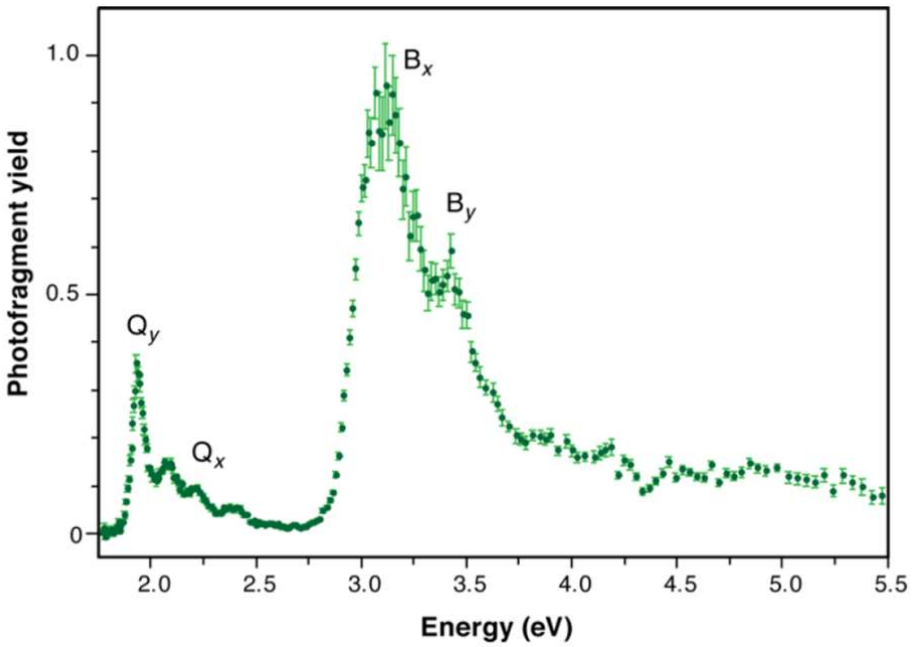

Figure 6: Gas-phase absorption spectrum of charge-tagged Chl a in the gas phase at 300 K after one-photon absorption.[42]

The absorption peaks of photopigments can be shifted by changing the energy of frontier orbitals via the functionalization of the central ring system or changing the central metal. The variety of different chlorophylls shows that on Earth the former method is preferred and many different sidechains are found on the central ring. However, other planets might substitute the metal center with other metals that show similar properties to Mg, like Zn or Ca.[26] Such metals are abundant in the Universe and could replace magnesium.[57]

When another metal is employed into the ring system the orbital energies experience a change due to the effect on the π-system.[40] If one assumes an idealized D_{4h} symmetry, the interaction of the metal with the a_{2u} orbital is restricted. Therefore, a metal with a higher electronegativity than magnesium will raise the orbital energy and a more electropositive metal will lower the energy of the orbital.[41]

1.4.2 Phot0

Phot0 is a primeval pigment introduced by Juan García de la Concepción *et al*., which could be a precursor for chlorophylls.[58] In their paper they provided a theoretical synthesis for the compound (Figure 7), as well as a substitution of the central metal ion with zinc Zn and magnesium Mg. Furthermore, they calculated reactive potential energy surfaces and UV/Vis spectra. These calculations utilized the density functional theory (DFT, explained in section 2.1), with the jun-cc-pVTZ basis set and a global-hybrid exchange-correlation MN15 method. The Zn complex was described by an effective-core potential LANL2DZ. For the UV/Vis spectra, the B2PLYP and the def2-TZVP basis set

were used on a CAM-B3LYP optimized geometry, including the dispersion correction D3(BJ). These methods were taken from the paper by Sirohwal *et al*., who built various derivates of Chl a intending to calculate their vibrionic transitions.[55] To obtain those they used the approach by Baiardi *et al*. and calculated their DLPNO-STEOM vertical excitation energies (VEEs), and transition dipole moments (TDMs) by using the Franck−Condon approximation (explained in section 1.5), and their derivatives (Herzberg−Teller effects). They calculated the ground- and excited-state geometries and the harmonic vibrational frequencies using the DFT/TD-DFT level.[55,59–62] After obtaining these results Sirohwal *et al*. compared the DLPNO−STEOM-CCSD to the literature values and DFT calculations. They found here that B2PLYP performed best.[55]

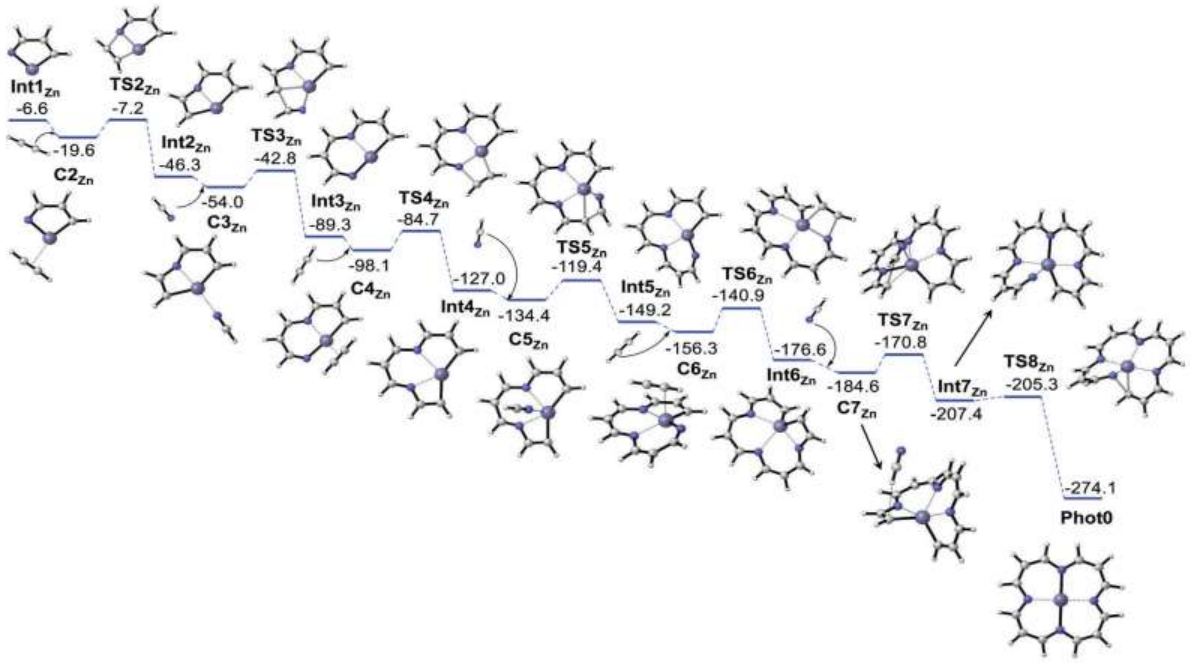

Figure 7: E + ZPE energy profiles showing the possible synthesis of Phot0 starting from Intermediate $Int1_{Zn}$ (energy values given in kcal mol^{-1}).[58]

In figure 8 the theoretical absorption spectrum for Chl a, BChl a, and two different Phot0 complexes is shown. As seen from the spectrum below the weakest absorption peaks of Phot0-Zn and Phot0-Zn are at 562 nm and 548 nm, which is close to the Q_y and Q_x bands respectively.

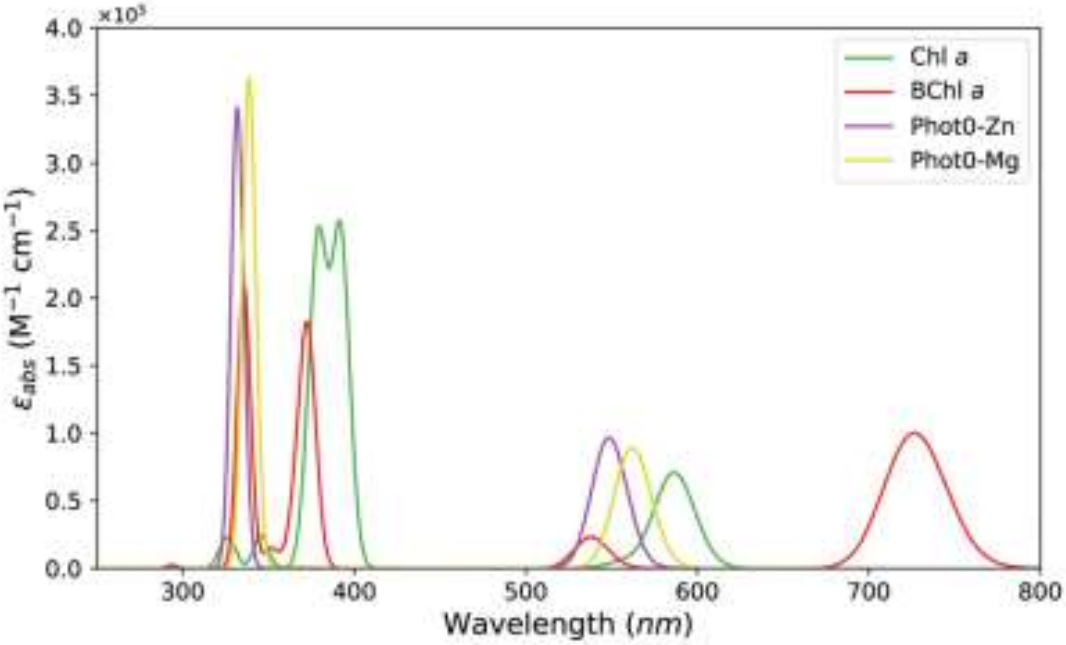

Figure 8: Theoretical UV/Vis absorption spectra of Chlorophyll a (green), Bacteriochlorophyll a (red), Phot0-Zn (purple), and Phot0-Mn (yellow) computed in vacuum and with a substitution of the phytyl groups in Chl a and BChl a with a methyl group.[58]

1.5 Vertical Excitation Energies and Frank-Condon principle

Most molecules show excited electronic states in addition to their ground electronic state. The ground state refers to the lowest energy state the molecule can have. If energy is absorbed an electron might jump from the ground state to a state with higher energy/ excited state. Those molecular electronic transitions are generally defined as the excitation of an electron from one energy level to a higher energy level, and therefore do not need to originate from the ground state.[63] One could for example imagine that the electron gets excited from the HOMO-1 to a higher energy level.

However, aside from just electronic transitions so called vibronic transition can occur. Vibronic transitions describe the combination of an electronic excitation combined with a vibrational excitation, which yields in vibrational fine structures observed in UV/Vis spectra. The absorbance of a photon can promote the molecule from its ground vibrational state to a higher vibrational level of an excited state.[63] The ground state, commonly referred to as X, and its energy (E_0 or E_g), can support many vibrational energy levels, however at sufficiently low temperatures (e.g. 0 K) the lowest vibrational level is the only populated one.[64] Therefore, electronic transitions originate from this vibronic level n=0. The excited state, usually called S_0 or S_1, is also able to support many vibrational levels, and, in addition, experiences a shift of the potential energy curve of nuclear coordinates. The potential energy curve is obtained from

calculations for the electronic structure of the molecule at particular coordinates and by solving for the eigenvalue of the energy (including potential and kinetic energy of electrons). Consequently, excitation into multiple different excited state levels is possible from the ground state (figure 9). The vibrational structure of electronic bands is defined by vibronic transitions, which occur when electronic and vibrational transitions happen simultaneously.[65] As a consequence vibrational fine structures play an important role in the characterization of energy transitions when observed in compounds. Vibronic structures can aid in line broadening because applicable molecules with vibrational modes will accompany electronic transitions and determine the line shape.[66]

The Frank-Condon principle states that the nuclear configuration shows no significant change during the energy absorption. This stems from the fact that the electron rearrangement is significantly faster than the motion of a nucleus (similar to the Born-Oppenheimer approximation).[65] Therefore, the electronic transitions happen on such fast timescales compared to the nuclei motion that the nuclei can be considered fixed during the transition. This means, that the nuclear coordinates (x-axis in figure 9) do not change during the electronic excitation and the excitation energies are consequently vertical (Vertical excitation energy, VEE).[63] The principle moreover states that the probability of every transition is defined by the degree of overlap occurring between the ground and excited state vibrational wave functions. Such individual vibrational bands are observable in gas phase absorption spectra of molecules, however the assignment to specific transitions is challenging.

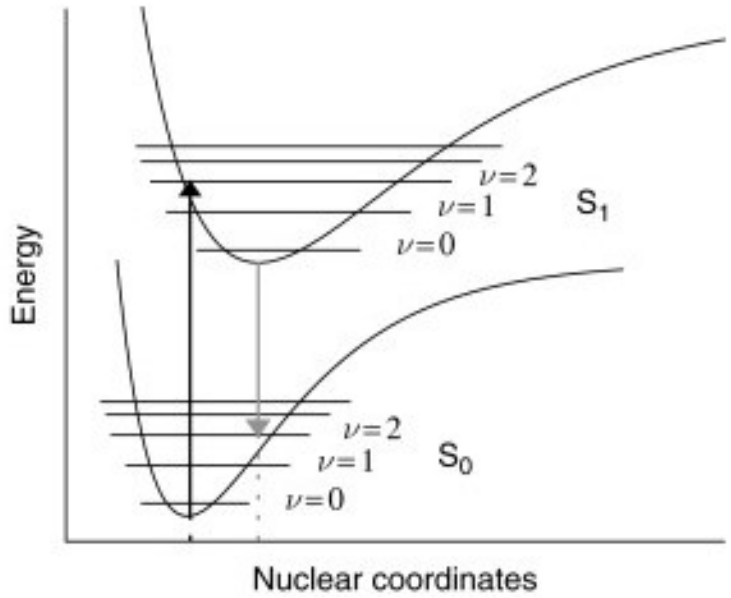

Figure 9: Franck-Condon principle: Graph of the molecular ground state potential energy curve, S_0, and molecular excited state potential energy curve, S_1, with their different vibrational levels (v).[63]

Chapter 2
Density Functional Theory

2.1 Density Functional Theory

Theoretical methods are able to bridge the gap between experimental data and fundamental physical principles, allowing the development of a deeper understanding of chemical systems. Over time various modeling approaches were developed, each with their own strengths and disadvantages. Earlier methods attempt to solve for the wavefunction, however the wavefunction´s unpredictability poses significant challenges and shows high computational cost. Striving to simplify this process the Density Functional Theory (DFT) was introduced, replacing the N-electron wavefunction with a much simpler model of the electron density $\rho(r)$.[67]

As previously mentioned, research groups modeled the absorption spectra of photopigments (Chl a and phot0) using mainly wave function theory (DLPNO STEOM CCSD). The results show high accuracy; however, this modelling is computationally cost-heavy, meaning that it takes a long time to finish the calculations. To reduce the computational cost density functional theory can be employed, which was shown by Sirohiwal *et al*.[55] They tested various DFT functionals and found that the B2PLYP functional shows a comparable accuracy to the WFT methods used. This work expands the benchmark of functionals to find more DFT functionals with comparable accuracy to the WFT standard.

The electron density is used to predict the behavior of electrons by solving the Schrödinger equation and was selected because density is a physical observable that is directly linked to the Hamiltonian *a priori*. The Hamiltonian operator is only dependent on the total number of electrons and the positions and atomic numbers of the nuclei. This information hints at the use of the electronic density to describe systems because the integration of the squared wavefunction over space yields the total number of electrons and therefore the electronic density.

2.1.1 Thomas-Fermi model

The Thomas-Fermi model was the first DFT model, developed in the 1920s, and is often used as a starting point for more advanced computational models.[67] The basic idea of this model revolves around the characterization of the electronic structure of a system being characterized solely by its electron density. The model assumes that electrons are delocalized and that there is an effective potential field that determines itself by the nuclear charge as well as the electron distribution.[67]

As already mentioned this model serves as a precursor for more complicated models, but shows several limitations. The Thomas-Fermi model is particularly restricted in the accurate description of electron

correlation effects. These issues stem from the fact that the kinetic energy is approximated and the correlation effect of electrons and the exchange energy of an atom is not represented in the model.

The exchange energy is a crucial term that needs to be defined better. Exchange energy, or exchange interaction, refers to an energy difference that stems from a difference in the configurations of electrons.[68] Since this definition is not trivial an example is introduced to help understand the exchange energy. One assumes a two-electron system with the two quantum states A and B, and the two electron spins α(parallel) and β(antiparallel). Here A_α would for example refer to quantum state A with parallel spins. There are two degenerate states (states of the same energy) called $A_\alpha B_\beta$ and $A_\beta B_\alpha$. If one combines these two states the following wavefunctions result:

$$\Psi_S = A_\alpha B_\beta + A_\beta B_\alpha$$

$$\Psi_A = A_\alpha B_\beta - A_\beta B_\alpha$$

These states are not degenerate anymore and the energy difference between E_S and E_A yields the exchange energy. Due to the difference in spin orientation, a variance in the electron configuration will be observed for Ψ_S and Ψ_A, because parallel electrons will avoid each other (Ψ_S) and *vice versa*.[68]

In 1930 Dirac improved the Thomas-Fermi model significantly by adding a term describing exchange energy, however, the issues with the kinetic energy still remained, making the method inaccurate for the description of molecular bonding.[69] Kohn and Sham were able to circumvent the problems caused by the kinetic energy by building a fictitious system with a known kinetic energy for non-interacting electrons.

2.1.2 Hohenberg-Kohn theorems

As explained earlier one of the biggest advantages of DFT is the replacement of the N-electron wavefunction with the electronic density, which is made possible by the Hohenberg-Kohn theorems. Instead of using orbital interpretations to describe the probability of electrons, DFT uses the "uniform electron gas" model or UEG model. The UEG´s main assumption is that electrons are uniformly distributed among the system, leading to homogeneous electron density throughout the material and an external potential interpreted as a uniformly distributed positive charge. The external potential that electrons experience can be more fittingly described as the nuclei attraction.

Now, the Hohenberg-Kohn Existence Theorem describes the ground-state density, which determines the external potential. To prove that the ground state density uniquely determines the external potential *reduction ad absurdo* is used. Firstly, we want to focus on the case that two different external potentials can be consistent with the same nondegenerate ground-state density ρ_0. The two potentials will be referred to as v_a and v_b, and their Hamiltonians respectively as H_a and H_b. A ground state wavefunction

Ψ_0 and eigenvalue E_0 are associated with each Hamiltonian. The variational theorem of molecular orbital theory states that the expectation value of Hamiltonian a over wavefunction b has to exceed the ground-state energy of a:

$$E_{0,a} < \langle \Psi_{0,b} | H_a | \Psi_{0,b} \rangle \quad (1)$$

This expression can be rewritten as follows:

$$\begin{aligned} E_{0,a} &< \langle \Psi_{0,\mathrm{b}} | H_a - H_b + H_b | \Psi_{0,\mathrm{b}} \rangle \quad (2) \\ &< \langle \Psi_{0,\mathrm{b}} | H_a - H_b | \Psi_{0,\mathrm{b}} \rangle + \langle \Psi_{0,\mathrm{b}} | H_b | \Psi_{0,\mathrm{b}} \rangle \\ &< \langle \Psi_{0,\mathrm{b}} | v_a - v_b | \Psi_{0,\mathrm{b}} \rangle + E_{0,b} \end{aligned}$$

The potentials v are one electron operators which means that the Eq. 2 can be integrated and written as follows:

$$E_{0,a} < \int [v_a(\boldsymbol{r}) - v_b(\boldsymbol{r})] \Psi_{0,\mathrm{a}}(\boldsymbol{r}) d\boldsymbol{r} + E_{0,b} \quad (3)$$

Since there is no difference between a and b the same applies to b and we can write the equivalent equation:

$$E_{0,b} < \int [v_b(\boldsymbol{r}) - v_a(\boldsymbol{r})] \Psi_{0,b}(\boldsymbol{r}) d\boldsymbol{r} + E_{0,a} \quad (4)$$

However, if inequalities are added to equations $E_{0,a}$ and $E_{0,b}$ we arrive at the following:

$$\begin{aligned} E_{0,a} + E_{0,b} &< \int [v_a(\boldsymbol{r}) - v_b(\boldsymbol{r})] \rho_0(\boldsymbol{r}) d\boldsymbol{r} + \int [v_b(\boldsymbol{r}) - v_a(\boldsymbol{r})] \rho_0(\boldsymbol{r}) d\boldsymbol{r} + E_{0,b} + E_{0,a} \\ &< \int [v_b(\boldsymbol{r}) - v_a(\boldsymbol{r}) + v_a(\boldsymbol{r}) - v_b(\boldsymbol{r})] \rho_0(\boldsymbol{r}) d\boldsymbol{r} + E_{0,b} + E_{0,a} \\ &< E_{0,b} + E_{0,a} \quad (5) \end{aligned}$$

This result is obviously impossible, since the sum of two energies cannot be less than itself, proving that the initial assumption was incorrect. It can be concluded that the external potential v is a unique functional, meaning that each density distribution has a unique potential energy. In other words, the nondegenerate ground-state density uniquely determines the external potential. The Hamiltonian can be replaced with the external potential because the kinetic energy operator remains unchanged and cancels out. It is evident that one realizes the direct influence that the external potential has on the Hamiltonian operator and the wavefunction.

This Existence theorem however is generally unhelpful to predict the density of a system and the total energy needs to be optimized. Therefore, Hohenberg and Kohn introduced their second theorem, the Variational Theorem, which aims to minimize the energy of the system by varying the electron density and thus determining the most stable electronic configuration (ground state). Hohenberg and Kohn assume that a candidate wavefunction Ψ_{cand} yields the correct number of electrons N upon integration.

$$\langle \Psi_{\text{cand}} | H_{cand} | \Psi_{\text{cand}} \rangle = E_{cand} \quad (6)$$

Utilizing the knowledge from the Existence theorem leads to the conclusion that such candidate wavefunctions and their Hamiltonians are "determined" by an electron density. The accompanying candidate energies E_{cand} can be only greater or equal to the true ground-state energy E_0:

$$E_{cand} \geq E_0 \quad (7)$$

2.1.3 Kohn-Sham Density Functional Theory

As explained in the Hohenberg-Kohn theorems the density determines the external potential and therefore influences the Hamiltonian and the wavefunction, enabling one to compute the energy.[70]

However, if one attempts to solve for the energy it is inevitable to solve the Schrödinger equation, which is prohibitively difficult, due to the electron-electron-interaction and the kinetic energy. Kohn and Sham came up with a solution to account for the kinetic energy and introduced the idea of an effective Hamiltonian, that describes a non-interacting system of electrons.[71] They picked a starting point for a system that is *fictitious,* with non-interacting electrons, while the overall ground-state density remains the same for electrons in real systems with interacting electrons.

In the Kohn-Sham density functional theory, the electronic energy is separated into five separate contributions:

$$E[\rho(\boldsymbol{r})] = T_{ni}[\rho(\boldsymbol{r})] + V_{ne}[\rho(\boldsymbol{r})] + V_{ee}[\rho(\boldsymbol{r})] + \Delta T[\rho(\boldsymbol{r})] + \Delta V_{ee}[\rho(\boldsymbol{r})] \quad (8)$$

The electronic energy consists of the non-interacting kinetic energy, $T_{ni}[\rho(\boldsymbol{r})]$, the electron-nuclear interaction energy, $V_{ne}[\rho(\boldsymbol{r})]$, the classical electron-electron repulsion, $V_{ee}[\rho(\boldsymbol{r})]$, the kinetic energy correction derived from the electron-electron interaction, $\Delta T[\rho(\boldsymbol{r})]$, and lastly the non-classical corrections to the electron-electron-repulsion energy, $\Delta V_{ee}[\rho(\boldsymbol{r})]$.[70,72]

For non-interacting electrons, the kinetic energy can be expressed as the sum of the individual electronic kinetic energies and the potential energy is ignored. Therefore, expressing the density via an orbital expression, Eq. 8 can be rewritten as follows:

$$E[\rho(\boldsymbol{r})] = \sum_i^N(\langle x_i| -\frac{1}{2}\nabla_i^2 \mid \mathrm{x_i}\rangle - \langle x_i|\sum_k^{nuclei}\frac{Z_k}{|\boldsymbol{r}_i-\boldsymbol{r}_k|}|\mathrm{x_i}\rangle) + \sum_i^N(\langle x_i \mid \frac{1}{2}\int\frac{\rho(\boldsymbol{r}')}{|\boldsymbol{r}_i-\boldsymbol{r}'|}d\boldsymbol{r}' \mid \mathrm{x_i}\rangle + E_{XC}[\rho(\boldsymbol{r})]) \quad (9)$$

Where N represents the number of electrons, x_i is the wavefunction of the i-th electron (also referred to as Kohn-Sham orbitals). These KS orbitals represent the distribution in space for one electron in the system and solve a single-electron Schrödinger-like equation. These wavefunctions were constructed according to the restricted Hartree-Fock (HF) theory[73,74] and produce the same electron density found in true interacting systems. (The HF method is used to approximate the electronic structure of many-body systems and generally assumes that a single Slater determinant is able to approximate the exact N-body wavefunction of a system. HF solves the Schrödinger equation by iteratively constructing an anti-symmetrized wavefunction that minimizes the total energy with respect to variations in orbital coefficients.[73,74]) The first term $\langle x_i| -\frac{1}{2}\nabla_i^2 \mid \mathrm{x_i}\rangle$ in Eq. 9 represents the kinetic energy contribution that the i-th electron has and is denoted by the kinetic energy operator ∇_i^2 acting on the electron wavefunction x_i. The second term $\langle x_i|\sum_k^{nuclei}\frac{Z_k}{|\boldsymbol{r}_i-\boldsymbol{r}_k|}|\mathrm{x_i}\rangle$ characterizes the contribution of the electron-nucleus interaction energy for the i-th electron. In the third term $\langle x_i \mid \frac{1}{2}\int\frac{\rho(\boldsymbol{r}')}{|\boldsymbol{r}_i-\boldsymbol{r}'|}d\boldsymbol{r}' \mid x_i\rangle$ the electron-electron interaction is described for the i-th electron, with the integral representing the classical electrostatic repulsion between the i-th electron and all other electrons in the system. Lastly, the non-classical contributions are accounted for in the fourth term $E_{XC}[\rho(\boldsymbol{r})]$,where E_{XC} is introduced as the so-called exchange-correlation energy. It is important to note that the two correction terms $\Delta T[\rho(\boldsymbol{r})]$ and $\Delta V_{ee}[\rho(\boldsymbol{r})]$ (Eq. 8) are combined in the exchange-correlation energy $E_{XC}[\rho(\boldsymbol{r})]$. The exchange-correlation energy includes the effects of quantum mechanical exchange of electrons, electron correlation, and corrections for the classical self-interaction energy, and the kinetic energy difference between the real and the fictitious non-interacting system.

The density ρ can be expressed by a Slater-determinantal wavefunction x_i, which is an exact eigenfunction of a non-interacting system:

$$\rho = \sum_{i=1}^N\langle x_i|x_i\rangle \quad (10)$$

The orbitals, that minimize the energy in eq 9, satisfy the pseudo eigenvalue equations:

$$h_i^{KS} x_i = \varepsilon_i x_i \quad (11)$$

One can further express the Kohn-Sham one-electron operator h_i^{KS} as follows:

$$h_i^{KS} = -\frac{1}{2}\nabla_i^2 - \sum_k^{nuclei} \frac{Z_k}{|\boldsymbol{r}_i - \boldsymbol{r}_k|} + \int \frac{\rho(\boldsymbol{r}')}{|\boldsymbol{r}_i - \boldsymbol{r}'|} d\boldsymbol{r}' + V_{XC} \quad (12)$$

Here V_{XC} is the exchange-correlation potential, which can be described as the functional derivative of E_{XC} over the density, expressing how the exchange-correlation energy changes when the density is varied:

$$V_{XC} = \frac{\delta E_{XC}}{\delta \rho} \quad (13)$$

The Hohenberg- Kohn theorems show that the external potential uniquely determines the ground state electron density and that a unique ground state density is obtained for any given external potential.[70,75] Following the logic of the Hohenberg-Kohn theorems, the XC energy is determined once the electron density is specified and a proper XC potential is specified.

Therefore, the total energy that is minimized (Eq. 9) is exact, which means that the minimum corresponds to the true ground state of the system.[70,75] Consequently, the KS orbitals x_i provide an exact density, because they are constructed to yield the electron density of the true interacting system. These orbitals form the Slater-determinantal eigenfunction for the non-interacting separable Hamiltonian, which is defined as the sum of the KS operators:

$$\sum_{i=1}^{N} h_i^{KS} |\mathrm{x}_1 x_2 \cdots x_N\rangle = \sum_{i=1}^{N} \varepsilon_i |\mathrm{x}_1 x_2 \cdots x_N\rangle \quad (14)$$

In conclusion it should be noted that the wavefunction in the KS approach is the Slater-determinantal eigenfunction and consists of the single-particle KS operators.

2.1.4 Exchange-correlation functionals

Exchange-correlation functions (XC functionals) can be roughly divided into three different categories: local functionals, hybrid functionals, and gradient-corrected functionals.[65] As established earlier, the XC energy E_{XC} includes the electron-electron repulsion and considers the kinetic energy difference between the real and fictitious non-interacting system.[70]

The exchange-correlation energy E_{XC} can be specified as the interaction of the electron density and the so-called exchange-correlation energy density, ε_{XC}:

$$E_{XC}[\rho(\boldsymbol{r})] = \int \rho(\boldsymbol{r})\varepsilon_{XC}[\rho(\boldsymbol{r})]dr \quad (15)$$

The energy density ε_{XC} can be expressed as the sum of individual correlation and exchange contributions:

$$\varepsilon_{XC}[\rho(\boldsymbol{r})] = \varepsilon_X[\rho(\boldsymbol{r})] + \varepsilon_C[\boldsymbol{r}_s] \quad (16)$$

In equation 16 ε_X represents the exchange, dependent on the density, and ε_C the correlation term, which is indirectly dependent on the density and directly dependent on the effective radius $\boldsymbol{r}_s$. The electron density can be expressed via a sphere, defined by an effective radius $\boldsymbol{r}_S$, which contains one electron exactly and has an evenly distributed density throughout.[70]

$$\boldsymbol{r}_S(\boldsymbol{r}) = \left(\frac{3}{4\pi\rho(\boldsymbol{r})}\right)^{\frac{1}{3}} \quad (17)$$

Equation 18 shows a general expression for the exchange energy density, which was approximated as follows:[70]

$$\varepsilon_X[\rho(\boldsymbol{r})] = -\frac{9\alpha}{8}\left(\frac{3}{\pi}\right)^{\frac{1}{3}}\rho^{\frac{1}{3}}(\boldsymbol{r}) \quad (18)$$

Here α is a coefficient that was empirically determined to fit known properties of systems.

2.1.5 Local Density Approximation

Historically, local density approximation (LDA) referred to density functionals that are able to compute the exchange-correlation energy at a given position *r* utilizing only the density ρ given at this position. For spin-unpolarized systems, one can approximate the exchange-correlation energy as such:

$$E_{XC}^{LDA}[\rho] = \int \rho(\boldsymbol{r})\varepsilon_{XC}\big(\rho(\boldsymbol{r})\big)d\boldsymbol{r} \quad (19)$$

With ε_{XC} representing the XC energy per particle in an UEG, while $\rho(\boldsymbol{r})$ indicates the electronic density at position $\boldsymbol{r}$. As the name implies the exchange-correlation energy consists of two terms, exchange and correlation:

$$E_{XC} = E_X + E_C \quad (20)$$

The UEG defines the exchange energy term as follows:

$$E_X^{UEG}[\rho(\boldsymbol{r})] = -\frac{9\alpha}{8}\left(\frac{3}{\pi}\right)^{\frac{1}{3}}\int \rho^{\frac{4}{3}}(\boldsymbol{r})d\boldsymbol{r} \quad (21)$$

However, the LDA does not assume a homogeneous density across the system and applies the UEG results to certain points in the room to derive the following expression:

$$E_X^{LDA}[\rho(\boldsymbol{r})] = -\frac{3}{4}\left(\frac{3}{\pi}\right)^{\frac{1}{3}} \int \rho^{\frac{4}{3}}(\boldsymbol{r}) d\boldsymbol{r} \quad (22)$$

The correlation term cannot be expressed in such a simple analytical form; however, one can make assumptions about the correlation energy for infinitively strong and weak correlations:

Attempting to get an analytical expression for the correlation energy Monte-Carlo calculations were carried out, yielding accurate results for correlation energy densities.[76] However, because the correlation term is not derived from its first principles many different approximations have been developed.

2.1.6 Generalized Gradient Approximation

The idea of the UEG was introduced earlier, however, the electron density in molecular systems usually does not resemble a uniform spatial distribution. The LDA describes the local environment and assumes a homogeneous electron density for this local environment, making it insufficient to describe larger molecular systems. First, note the spin-dependent time dependent density functional theory (TDDFT, section 2.2) version derived by Liu and Vosko.[77] DFT is limited to the description of the ground state of molecules, while TDDFT provides information about excited states. The time dependent part of the density $\rho(\boldsymbol{r}, t)$, is developed from the ground state and created under the influence of an external time-dependent field $\lambda_{vext}(\boldsymbol{r}, t)$. Consequently, the wave function can be described as a functional of the density (more detailed explanation is in section 2.2).[78] Historically, the local density approximation (LDA) was the first XC functional developed in ground-state DFT.[76] The LDA approximates the XC density at each point in space via the XC energy density of an electron gas of homogeneous nature.[71]

$$E_{XC}^{LDA}[\rho] = \int d^3\boldsymbol{r}\rho(\boldsymbol{r}) e_{XC}^{UEG}(\rho) \quad (23)$$

The potential in the LDA is local and therefore the potential value at a position $\boldsymbol{r}$ solely depends on the spin density value at the same point. To advance the correlation functional and to consider long range correlations a gradient correction is added, hence the name Generalized Gradient Approximation, GGA. Most of the time this gradient term is added to the LDA functional as follows:

$$\varepsilon_{XC}^{GGA}[\rho(\boldsymbol{r})] = \varepsilon_{XC}^{LDA}[\rho(\boldsymbol{r})] + \Delta\varepsilon_{XC}\left[\frac{|\nabla\rho(\boldsymbol{r})|}{\rho^{\frac{4}{3}}(\boldsymbol{r})}\right] \quad (24)$$

The gradient is also expressible as follows:[79]

$$E_{XC}^{GGA}[\rho] = \int d^3\boldsymbol{r}\rho(\boldsymbol{r}) e_{XC}^{GGA}(\rho, \Delta\rho) \quad (25)$$

Becke developed the first and very popular GGA functional, which is commonly abbreviated with just the letter "B". This functional was constructed to accurately describe asymptotic behavior for the long-range correlations of the energy density. Becke included a correction parameter into the functional that was obtained empirically by fitting to the exchange energies of six noble gases.[80]

Aside from Becke, scientists like Perdew and Wang, as well as Langreth and Mehl paved the path for the GGA. They published popular GGAs, such as Becke´s B88 functional, an asymptotically correct exchange functional, or the PBE functional, which was introduced by Perdew, Burke, and Ernzerhof.[81] The PBE functional is a constraint-selection-based functional, meaning that the functional was constructed under consideration of specific constraints and eventually build by selecting the functional that best satisfied the requirements.[82]

However, GGAs are limited by their construction and no GGA functional is able to "*satisfy all the theoretical constraints of the exact functional*"[82], meaning that it cannot capture the entirety of the electron-electron interactions and correlation effects. Examples of select constrains are for example extreme (high or low) densities, dispersion interactions, or accurate description of correlation effects.[83]

To solve this issue, Perdew *et al*. proposed a more general class of functionals called meta-GGAs, implementing the kinetic energy density τ_σ:[84]

$$E_{XC}^{MGGA}[\rho] = \int d^3\boldsymbol{r}\rho(\boldsymbol{r})e_{XC}^{GGA}(\rho, \nabla\rho, , \nabla^2\rho, \tau) \quad (26)$$

$$\tau_\sigma(\boldsymbol{r}) = \sum_i^{occupied} \frac{1}{2}|\nabla x_i(\boldsymbol{r})|^2 \quad (27)$$

with x_i representing KS orbitals.

2.1.7 Hybrid Density Functionals

Hybrid exchange-correlation (XC) functionals significantly improved the description of molecules.[85] They approximate the XC energy functional "mixing" exact exchange with other *ab inito* or empirical XC energies:

$$E_{XC}^{hybr} \quad [\rho(\boldsymbol{r})] = \alpha E_X^{HF}[\rho(\boldsymbol{r})] + (1-\alpha)E_{XC}^{DFT}[\rho(\boldsymbol{r})] \quad (28)$$

Where $E_X^{HF}[\rho(\boldsymbol{r})]$ resembles the exchange energy from the Hartree-Fock theory, $E_{XC}^{DFT}[\rho(\boldsymbol{r})]$ is the exchange and correlation energy from standard DFT functionals, and α is a mixing parameter, determining the fractions of HF and DFT exchange in the hybrid functional.[70] HF exchange, or exact exchange, is used to improve the description of electronic properties, like charge transfer (CT) transitions, which are defined as transitions occurring between an electron donor and an electron

acceptor.[86] It is well known that excitation energies for long-range transitions in CT states are underestimated in TDDFT (section 2.2) and the wrong asymptotic behavior is given for the potential energy curves of these CT states.[87] By adding exact exchange the correct 1/R long-range behavior is observed for the potential energy surface (here R represents the distance between two charges in a CT state). The paper by Dreuw and Head-Gordon provides a detailed explanation how HF fixes the self-interaction error that is encountered if pure XC-functionals are used and explores how HF fixes these issues.[87]

There are two different ways exact exchange can be incorporated into hybrid functionals: range separated or global.

Global functionals are designed to accurately replicate the modified fourth-order expansion of the exchange energy. This expansion can be applied in the semiclassical limit to neutral and many-electron atoms. Additionally, this approximation aims to restore the complete local density approximation linear response.[88] Global hybrid functionals are describable as hybrid versions of the APBE functional, which was introduced in 2011 by Constantin et al.[89] Another correlation functional is added to localize the correlation energy density. This modification results in enhanced compatibility with the Hartree-Fock exchange and the coupling-constant-resolved XC potential energy.

As for the construction of the hybrid functionals, one starts by defining the exchange-correlation functional, which is given by the coupling-constant integration formula

$$E_{XC} = \int_0^1 W_{XC,\lambda}\, d\lambda \qquad (29)$$

The appropriate coupling-constant-resolved XC potential energy $W_{XC,\lambda}$ is often expressed by the ansatz by Perdew, Ernzerhof, and Burke.[81] In the equation below DFA refers to local or semilocal density approximation:

$$W_{XC,\lambda} = W_{XC,\lambda}^{DFA} + \left(E_X^{HF} - E_X^{DFA}\right)(1-\lambda)^{n-1} \qquad (30)$$

Here, $W_{XC,\lambda}^{DFA}$ refers to the XC potential energy in DFA, while E_X^{HF} and E_X^{DFA} represent the classical HF and semilocal DFA exchange energies. This equation yields exact exchange only when $\lambda = 0$ and the assumption stands that $W_{XC,1}$ is accurately approximated by DFA.[90] Combining equations 29 and 30 gives:

$$E_{XC} = \frac{1}{n}E_X^{HF} + \left(1 - \frac{1}{n}\right)E_X^{DFA} + E_X^{DFA} \qquad (31)$$

2.1.8 Range-Separated Hybrid Functionals

Range-separated hybrid functionals (RSH) count towards the nonlocal exchange functionals.[91] These functionals are constructed to focus on a local environment and a long-range environment of the density. Head-Gordon *et al.* use the B97 density functional, which is produced by combining exchange functionals and spin correlation functionals:[91]

In general, local exchange, global hybrid, and range-separated hybrid functionals can be constructed from the following three equations:

First and foremost, as stated before, the exchange-correlation energy E_{XC} is a combination of correlation and exchange energy:

$$E_{XC} = E_X + E_C \quad (32)$$

In the equation below "sr" refers to "short range" and "lr" to "long-range", while "os" stands for "opposite spin", and lastly "ss" for "same spin".[92]

$$E_X = E_X^{B97} + c_x E_{x,sr}^{exact} + d_x E_{x,lr}^{exact} \quad (33)$$

$$E_C = E_{c,ss}^{B97} + E_{c,os}^{B97} + E_{disp} \quad (34)$$

For range-separated hybrid functionals $d_x = 1$ and E_X^{B97} is defined by the long-range and short-range energies $E_{X,sr}^{exact}$ and $E_{X,lr}^{exact}$.[93,94]

The main difference between RSH functionals and global hybrid functionals is that for GH $c_X = d_X$, where c_X can be described as the global fraction of exact exchange. For RSH, $d_x = 1$, whereas c_x is allowed to be independent of d_x.

2.1.9 Domain-based local pair natural orbital implementation of the equation of motion coupled cluster method

Accurate calculations of excited states are of enormous importance and can be achieved in various ways, common methods include for example the complete active space second-order perturbation theory (CASPT2) or TDDFT (section 2.2).[95] Another method, called the single reference coupled cluster theory, can be generalized to excited states by using the equation of motion (EOM) approach, developed by Rowe *et al.* in 1968.[96–98] The equation of motion coupled cluster method (EOM-CC) is generally employed for singles and doubles coupled cluster amplitudes (EOM-CCSD) and predicts excitation energies sufficiently accurate for single excitation dominated states.[98–100]

However, one big disadvantage of EOM-CCSD is the size limitation of molecules, due to the N^6 scaling (N indicating the number of basis sets in the system) and its associated storage requirements. The literature describes different approaches to reduce the EOM-CCSD scaling, however, this thesis will highlight the so-called STEOM approach.[101]

Nooijen *et al.* formulated the similarity transformed equation of motion (STEOM) method which can efficiently describe charge transfer (CT) states.[102,103] STEOM is a similarity transformation that is parameterized by the ionization potential (IP) and the electron affinity (EA) solutions of the equation of motion (EOM) approach.[101] This is applied to the CCST (coupled cluster with single and triple excitations) Hamiltonian to decouple singles and doubles. Once diagonalized in the single excitation space, the Hamiltonian can yield size-extensive excitation energies. In 2013 Neese *et al.* introduced the domain-based pair natural orbitals (DLPNO) theory which prolongs this method and enables the highly accurate calculation of excited state energies of larger molecules.[101,104,105]

The combination of these schemes also called the DLPNO-STEOM-CCSD method, is able to describe higher-order excitations (singles and double excitations) and additionally contains a triple excitation effect through the linked connections, which makes it a robust tool to reproduce accurate excited state properties.[106–110]

2.2 Time-Dependent Density Functional Theory

The foundation for modern time-dependent density functional theory was laid in 1984 by Runge and Gross by deriving a theorem similar to Hohenberg-Kohn´s theorem for the time-dependent Schrödinger equation.[111] DFT and TDDFT methods both are formally exact theories and their accuracy is dependent on the correctness of the exchange-correlation (XC) functionals.

TDDFT is a very popular method to calculate excited states of medium to large molecules, such as biomolecules. However, XC functionals tend to have an approximate nature which limits the accuracy of results like Rydberg states, charge-transfer states, large π-systems, and doubly excited states. These limitations can mostly be attributed to self-interaction errors, which are weakened if one includes a percentage of exact exchange with range-separated or global-hybrid functionals. Previous attempts to introduce exact exchange with the help of these functionals proved to be unsuccessful.

To accurately describe the electronic spectra of molecules one needs to know about the energetic configurations of excited states with respect to the ground state and additionally about the excited states' geometry and electronic properties. Due to excitation from the ground state into electronically higher excited levels the electronic many-body wavefunction changes. To analyze the electronic transition, one needs to investigate the change in the wavefunction first. The analysis of this change is done by applying

principles used to analyze the ground state to the excited state. Firstly, DFT is used to calculate the initial Kohn-Sham (KS) orbitals. These orbitals represent the exact density of the true ground state, which moreover represents the initial state of the TDDFT calculations. Afterward, time-independent DFT exchange-correlation (XC) functionals used in the ground state are utilized to carry out the TDDFT calculations.

2.2.1 Theory behind TDDFT

Starting with some preliminaries, we review systems described by the nonrelativistic many-body Schrödinger equation:

$$i\frac{\partial}{\partial t}\Psi(\boldsymbol{r},t) = \hat{H}(\boldsymbol{r},t)\Psi(\boldsymbol{r},t) \quad (35)$$

Here $\hat{H}$ is the Hamiltonian operator of the system and the electrons are described by their spatial coordinates $\{\boldsymbol{r}\} = \{r_1, \cdots, r_N\}$, with $\{\boldsymbol{r}\}$ being a collection of all r´s. By employing equation 35 one can calculate Ψ at any time *t*, under the condition that the initial state of the system at an initial time t_0 is known. The difference to the time-independent Schrödinger equation is evident since our aims are substantially different. In the time-independent case, we want to find eigenstates of the Hamiltonian that fulfill appropriate boundary conditions. The Hamiltonian operator consists of three different parts:

$$\hat{H}(\boldsymbol{r},t) = \hat{W}(\boldsymbol{r}) + \hat{T}(\boldsymbol{r}) + \hat{V}_{ext}(\boldsymbol{r},t) \quad (36)$$

$\hat{W}(\{\boldsymbol{r}\})$ refers to the electron-electron interaction and $\hat{T}(\{\boldsymbol{r}\})$ stands for the kinetic energy:

$$\hat{T}(\{\boldsymbol{r}\}) = -\frac{1}{2}\sum_{i=1}^{N}\nabla_i^2 \quad (37)$$

$$\hat{W}(\{\boldsymbol{r}\}) = \frac{1}{2}\sum_{\substack{i,j=1\\ i\neq j}}^{N}\frac{1}{|\mathbf{r}_i-\mathbf{r}_j|} \quad (38)$$

The last term $\hat{V}_{ext}(\{\boldsymbol{r}\},t)$ is expressable as the sum of one-body potentials and describes for example Coulomb interactions of a total number of electrons *N* with a total number of nuclei N_n:

$$\hat{V}_{ext}(\{\boldsymbol{r}\},t) = \sum_{i=1}^{N} v_{ext}(\boldsymbol{r}_i,t) \quad (39)$$

$$v_{ext}(\boldsymbol{r}_i,t) = -\sum_{v=1}^{N_n}\frac{Z_v}{|\mathbf{r}_i-\mathrm{R}_v(t)|} \quad (40)$$

Z_v denotes the charge and R_v gives the position of the nucleus v. Next, we want to focus on the wave function Ψ, specifically on the absolute square of Ψ, which gives the probability of finding electrons at specific positions $\boldsymbol{r}_i$ at a given time t. Based on this we can write eq 41, which visualizes the normalized density $\rho(\boldsymbol{r},t)$ calculated by multiplying the probability by N to obtain an electron at position $\boldsymbol{r}$ and time t.[79]

$$\rho(\boldsymbol{r},t) = N \int d^3\boldsymbol{r}_2 \cdots d\boldsymbol{r}_N^3 \, |\Psi(\boldsymbol{r}_1, \boldsymbol{r}_2 \cdots \boldsymbol{r}_\mathrm{N}, \mathrm{t})|^2 \quad (41)$$

2.2.2 Runge-Gross-Theorem

The main theorem of TDDFT, also referred to as Runge-Gross-Theorem, proves that for many-body systems, originating from a fixed initial state, a one-to-one correspondence between an external potential $v_{ext}(\boldsymbol{r}_i, t)$ and the electronic density $\rho(\boldsymbol{r}, t)$ is found.[111] Therefore, if the density is known for a fixed initial state we can calculate the external potential and thus solve the time-dependent Schrödinger equation to solve for all other properties. If the system differs from the ground state however, for example through excitation, the situation changes and the initial state needs to be known/ obtained.[112–114]

Utilizing the Runge-Gross scheme to construct a time-dependent KS scheme is rather straightforward. Firstly, we use an auxiliary system of noninteracting electrons which are subject to a local external potential v_{KS}.[79] This potential v_{KS} is unique and chosen to match the density of the KS electrons with the density in the initial interacting system. The KS electrons obey the earlier introduced time-independent Schrödinger equation:

$$i\frac{\partial}{\partial t}\Psi_i(\boldsymbol{r},t) = \hat{H}_{KS}(\boldsymbol{r},t)\Psi_i(\boldsymbol{r},t) \quad (42)$$

Kohn-Sham Hamiltonian is expressed as

$$\hat{H}_{KS}(\boldsymbol{r},t) = -\frac{\nabla^2}{2} + v_{KS}[\rho](\boldsymbol{r},t) \quad (43)$$

The density of the interacting system can be obtained by calculating the Kohn-Sham orbitals

$$\rho(\boldsymbol{r},t) = \sum_i^N |\Psi_\mathrm{i}(\boldsymbol{r},t)|^2 \quad (44)$$

Analogous to the Kohn-Sham ground state we express the time-dependent KS potential as follows:

$$v_{KS}[\rho](\boldsymbol{r},t) = v_{ext}(\boldsymbol{r},t) + v_{Hartree}[\rho](\boldsymbol{r},t) + v_{XC}[\rho](\boldsymbol{r},t) \quad (45)$$

The first two terms are known, with $v_{ext}(\boldsymbol{r},t)$ being the external potential and $v_{Hartree}[\rho](\boldsymbol{r},t)$ the classical electrostatic interaction of electrons, defined as:

$$v_{Hartree}(\boldsymbol{r},t) = \int d^3\acute{r}\frac{\rho(\boldsymbol{r},t)}{|\boldsymbol{r}-\acute{\boldsymbol{r}}|} \quad (46)$$

The third term in eq 48 $v_{XC}[\rho](\boldsymbol{r},t)$ is called xc potential and includes all nontrivial many-body effects and is essentially unknown due to the density dependence. We deal with a nonlocal dependence on space

and time, which means that the potential depends on the density at all prior times and positions due to causality.[79] The KS potential is calculated by using the two known terms (external and Hartree potential) and approximating the XC potential.

The quality of the results is highly dependent on the approximations of the xc potential, which is approximated by several different mathematical and physical tactics. Like in the ground-state DFT this is the only fundamental approximation for TDDFT.[79]

2.2.3 Tamm-Dancoff approximation

In 1945 Igor Yevgenyevich Tamm introduced a new approximation method in his paper for many-body physics, which was later developed by Sidney Dancoff in 1950.[115,116] Head-Gordon applied these principles to quantum mechanics, which is known today as the Tamm-Dancoff-approximation.[117] This approximation has a significant influence on the computational cost and accuracy of TDDFT calculations. To understand how the approximation works one needs to analyze the real Kohn-Sham orbitals in TDDFT:

$$\begin{pmatrix} A & B \\ B & A \end{pmatrix}\begin{pmatrix} X \\ Y \end{pmatrix} = \omega \begin{pmatrix} 1 & 0 \\ 0 & -1 \end{pmatrix}\begin{pmatrix} X \\ Y \end{pmatrix} \quad (47)$$

With ω representing the excitation energies and X and Y being "*virtual–occupied and occupied–virtual elements*".[117] These real KS orbitals show the form of a non-Hermitian eigenvalue problem, the specific definition of the A and B matrices elements can be found in the paper by Dreuw and Head-Gordon or Hirata and Head-Gordon.[87,117]

The Tamm-Dancoff approximation essentially neglects the B-matrix, meaning the deexcitation amplitudes in the time-dependent density functional theory eigenvalue problem are not considered.[87,117]

2.2.4 Drawbacks of TDDFT

Even though TDDFT is the usual go-to method to compute absorption spectra of medium and large molecules, the theory has some major drawbacks. Approximated TDDFT functionals do not provide accurate results for CT states, yielding in blue-shifted Gouterman state energies and formation of ghost-states, which are overstabalized non-Gouterman states.[40] The excitation energy of charge transfer (CT) states, which is determined by the difference between donating and accepting orbital energies under a pure XC functional, leads to potential energy curves lacking the correct 1/R behavior.[87] This problem of TDDFT with standard XC functionals to yield the correct 1/R behavior stems from a self-interaction error.[87] However, using nonlocal HF exchange or hybrid functionals improves the asymptotic behavior.

Chapter 3
Results

3.1 Results

3.1.1 TDDFT calculations for chlorophyll a absorption spectra

The goal of this work was to expand the benchmark of approximations, like modern exchange-correlation approximations, on absorption spectra of selected photopigments. The quasi-experimental results obtained and published by Sirohiwal *et al*. were used as the most accurate benchmark for Chl a.[55] In addition to that, a potential photopigment precursor, called phot0, was analyzed utilizing the DLPNO-STEOM-CCSD (section 2.1.9) to generate data for molecules with unavailable experimental spectra. Since previous attempts failed to include exact exchange with global- or range-separated hybrid functionals (section 2.1.7 and 2.1.8) for Chl a, this work employed previously untested exchange-correlation functionals (section 2.1.4) with an emphasis on range-separated functionals. Previous work has shown that absorption spectra for Chl a can be computed with high accuracy using methods like the SAC-CI, CC2, and ADC(2), however these methods have a high computational cost.[43,47,118] The only TDDFT (section 2.2) functional, a double hybrid functional called B2PLYP, able to provide an accurate one-stop-solution for every low-energy feature in the absorption spectrum of Chl a. Therefore, our particular goal was to compare the performance of modern functionals that have the potential to yield results comparable to the B2PLYP functional, but with a lower computational cost.

The TDDFT calculations were performed utilizing the def2-TZVP basis set and 25 functionals that have not been tested previously in the literature. To perform the calculations the Q-Chem 6.1 program was used. Functionals, known to work well for many properties in addition to all available range-separated hybrids were tested.[91,119–124] The gas-phase molecular geometry was calculated according to Sirohiwal *et al.*[55] using CAM-B3LYP-D3(BJ)/def2-TZVP, which replaces the phytyl chain found at position 17 in Chlorophyll a with a methyl group. This optimization guarantees the smallest geometry chlorophyll a can realize containing 73 atoms. For the integration of the exchange-correlation energies, the "ultrafine" Lebedev grid of 99 radial and 590 angular points was applied. To guarantee that both bands (Q- and B-band) are covered in the calculation the number of states was varied depending on the functional type and starting geometry. For hybrid functionals, a minimum of 10 states were required when the CAM-B3LYP-D3(BJ)/def2-TZVP was used and a maximum of 20 states were required to carry out a calculation with local functionals and the xtb geometry. The results for the VEE of the B- and Q-bands of Chl a are presented in Table 1 below.

Table 1: Vertical Excitation energies (in eV) related to the Q- and B-bands of Chl a calculated with the DLPNO-STEOM-CCSD and TD-DFT. The obtained values are compared to quasi-experimental VEEs found in Sirohiwal *et al*.[55] The results in the table were obtained from the paper by Illner *et al*.[40]

[2]**Method:**	**Type**[a]	**Reference**	Q_y	Q_x	B_x	B_y
Quasi-experimental		[55]	1.99 (1)	2.30 (2)	3.12 (3)	3.38 (4)
DLPNO-STEOM-CCSD	WFT	[125–127]	1.75 (1)	2.24 (2)	3.17 (3)	3.40 (4)
TD-HF/RPA	WFT	[128,129]	2.05 (1)	3.22 (2)	3.89 (3)	4.52 (5)
CIS	WFT	[130,131]	2.45 (1)	3.48 (2)	4.29 (3)	4.84 (6)
CIS(D)	WFT	[132,133]	2.16 (1)	2.23 (2)	3.12 (3)	3.34 (4)
BLYP	L	[80,134]	2.05 (1)	2.13 (2)	2.82 (6)	2.95 (7)
PBE	L	[81]	2.07 (1)	2.14 (2)	2.83 (6)	2.96 (7)
BP86	L	[80,135]	2.06 (1)	2.14 (2)	2.84 (6)	2.96 (7)
M06-L	L	[136]	2.13 (1)	2.24 (2)	3.01 (6)	3.15 (7)
MN15-L	L	[120]	2.23 (1)	2.38 (2)	3.17 (6)	3.34 (7)
TPSS	L	[137]	2.09 (1)	2.18 (2)	2.90 (6)	3.03 (7)
SCAN	L	[138]	2.13 (1)	2.24 (2)	3.02 (6)	3.15 (7)
r^2SCAN	L	[139]	2.16 (1)	2.26 (2)	3.01 (6)	3.15 (7)
B97M-V	L	[140]	2.15 (1)	2.28 (2)	3.05 (6)	3.20 (7)
B3LYP	GH (20%)	[80,134,141]	2.16 (1)	2.35 (2)	3.17 (4)	3.35 (7)
PBE0	GH (25%)	[142]	2.19 (1)	2.40 (2)	3.26 (4)	3.45 (7)
TPSSh	GH (10%)	[143]	2.16 (1)	2.29 (2)	3.09 (6)	3.24 (7)
r^2SCANh	GH (25%)	[144]	2.20 (1)	2.35 (2)	3.17 (6)	3.33 (7)
r^2SCAN0	GH (25%)	[144]	2.24 (1)	2.47 (2)	3.36 (4)	3.56 (6)
PW6B95	GH (28%)	[145]	2.17 (1)	2.40 (2)	3.22 (3)	3.27 (4)
M06	GH (27%)	[146]	2.11 (1)	2.35 (2)	3.23 (4)	3.42 (7)
M06-2X	GH (54%)	[146]	2.19 (1)	2.56 (2)	3.44 (3)	3.69 (5)
M08-HX	GH (52%)	[147]	2.21 (1)	2.56 (2)	3.44 (3)	3.68 (5)
M08-SO	GH (57%)	[147]	2.15 (1)	2.54 (2)	3.41 (3)	3.68 (5)
MN15	GH (44%)	[148]	2.15 (1)	2.47 (2)	3.33 (3)	3.56 (6)
LC-ωPBE	RSH (0–100%)	[149]	2.07 (1)	2.59 (2)	3.47 (3)	3.78 (5)
LC-ωPBEh	RSH (20–100%)	[150]	2.12 (1)	2.54 (2)	3.44 (3)	3.73 (5)
CAM-B3LYP	RSH (19–100%)	[151]	2.14 (1)	2.53 (2)	3.43 (3)	3.71 (5)
ωB97M-V	RSH (15–100%)	[152]	2.06 (1)	2.64 (2)	3.49 (3)	3.85 (5)
ωB97X-V	RSH (17–100%)	[92]	2.07 (1)	2.68 (2)	3.54 (3)	3.91 (5)
M11	RSH (43–100%)	[153]	2.11 (1)	2.67 (2)	3.52 (3)	3.86 (6)
revM11	RSH (23–100%)	[154]	2.02 (1)	2.75 (2)	3.52 (3)	3.89 (5)
ωB97X-D	RSH (22–100%)	[155]	2.12 (1)	2.55 (2)	3.45 (3)	3.75 (5)
ωB97X-D3	RSH (20–100%)	[156]	2.09 (1)	2.61 (2)	3.50 (3)	3.83 (5)
ωM05-D	RSH (37–100%)	[157]	2.11 (1)	2.59 (2)	3.47 (3)	3.78 (5)
ωM06-D3	RSH (27–100%)	[156]	2.08 (1)	2.69 (2)	3.55 (3)	3.88 (4)
B2PLYP	DH	[158]	2.12 (1)	2.23 (2)	3.17 (3)	3.27 (4)
ωB2PLYP	RS-DH	[159]	2.04 (1)	2.49 (2)	3.45 (3)	3.78 (4)

[a]WFT refers to Wave Function Theory, where L denotes Local, GH indicates Global-Hybrid, RSH stands for Range-Separated–Hybrid, DH represents Double-Hybrid, and RS-DH signifies Range-Separated Double Hybrid. For GH and RSH functionals, the percentage of exact exchange is additionally provided in parentheses.[40]

As explained in the introduction (Chapter 1) one needs to specifically focus on the Q-band when investigating photopigments of exoplanetary interest since the Q-band is directly linked to the VRE. Therefore, three statistical indicators were designed to assess the performance of TD-DFT calculations. Firstly, as indicated earlier, we focused on the performance of the Q-band and assigned a mean unassigned error (MUE) called Q-MUE. Secondly, the performance of the other band, B-band, was assessed and B-MUE was calculated with respect to Siohiwal´s quasi-experimental VEEs.[55] For the last indicator we looked at the presence of "ghost-states" between the B- and Q-band. Such states complicate the assignment or interpretation of peaks, thus it is favorable to have a low number of GS in the spectrum. They occur as a result of overstabilization by a wrong asymptotic form of the exchange-correlation potential. To calculate the #GS indicator the average number of non-Gouterman states is taken in the region between the Gouterman energies.

All three indicators were combined to calculate the weighted mean unassigned error (wMUE) as follows:

$$wMUE = w_Q QMUE + w_B BMUE + w_G \#GS \quad (48)$$

The weights of the different indicators were chosen based on their qualitative ranking in an astrochemical context. We chose w_Q to equal 1 because it determines the position of the Q-band and therefore the postion of the VRE, w_B is chosen to be 0.5, while w_G is specified to be 0.1 because these states complicate the interpretation of the spectrum but otherwise do not influence the peak positions of the Q or B-band negatively.

The results indicate that four methods performed significantly better than all other tested methods. The four functionals are: CIS(D) wave function theory methods, B2PLYP double hybrid functional, DLPNO-STEOM-CCSD wave function method, and lastly the PW6B95 global-hybrid functional. CIS(D) showed a slightly better performance than B2LYP and DLPNO-STEOM-CCSD, which have been highlighted in previous literature as the "best" methods for computation of Chl a.[55] The slight performance advantage of CIS(D) stems from an optimal description of the B-band. B2PLYP performs slightly better than DLPNO-STEOM-CCSD, which is interesting since DLPNO-STEOM-CCSD is a highly accurate method. Both wavefunction methods have trouble describing the Q_y band. Cis(D) shifts it by 0.16 eV in the blue region, while the Q_y band experiences a red shift by 0.24 eV if calculated with DLPNO-STEOM-CCSD. All other transitions are described more accurately by the wave function methods.

Table 2 shows the MUEs for the Q-, and B-bands, as well as the number of GS and total MUE for every method. The results demonstrate that most density functionals show Q-MUEs lower than 0.15 eV, proving TDDFT calculations to generally be reliable for low-lying energy states. Among those were mostly local and global hybrid functionals with a low to moderate fraction of exact exchange, however, such functionals over-stabilize CT ghost states quite substantially leading to a high #GS. Moreover, local functionals are generally unreliable for the description of the B-band. Lowering self-interaction errors by the employment of higher percentages of exact exchange or range-separation cuts both ways.[40]

Table 2: Overview over all tested methods and their mean unassigned errors (MUEs) for Chl a. The errors were calculated with respect to the quasi-experimental vertical excitation energies (VEES) reported by Sirohiwal et al.[55] Three statistical indicators were used to calculate the weighted MUE (wMUE): MUE for the peak positions of the Q-band; B-MUE: MUE for the peak positions of the B-band; #GS: average number of 'ghost states' between the Q- and B-band. The color scheme indicated the performance with decreasing accuracy from green (best) to red (worst).[40] Table 1 contains the abbreviations used for the functional types.

Method	Type	Q-MUE	B-MUE	#GS	wMUE
CIS(D)	WFT	0,12	0,02	0	0,129
B2PLYP	DH	0,10	0,08	0	0,140
DLPNO-STEOM-CCSD	WFT	0,15	0,03	0	0,168
PW6B95	GH (28%)	0,14	0,11	0	0,194
ωB2PLYP	RS-DH	0,12	0,37	0	0,303
M06	GH (27%)	0,09	0,08	2	0,323
B3LYP	GH (20%)	0,11	0,04	2	0,328
MN15	GH (44%)	0,16	0,20	1	0,362
M08-SO	GH (57%)	0,20	0,29	0,5	0,395
CAM-B3LYP	RSH (19–100%)	0,19	0,32	0,5	0,401
PBE0	GH (25%)	0,15	0,10	2	0,401
LC-ωPBEh	RSH (20–100%)	0,18	0,33	0,5	0,402
ωB97X-D	RSH (17–100%)	0,19	0,35	0,5	0,411
LC-ωPBE	RSH (0–100%)	0,18	0,37	0,5	0,421
TPSSh	GH (10%)	0,09	0,08	3	0,430
M06-2X	GH (54%)	0,23	0,32	0,5	0,436
M08-HX	GH (52%)	0,24	0,31	0,5	0,444
ωM05-D	RSH (37–100%)	0,21	0,38	0,5	0,446
B97M-V	L	0,09	0,12	3	0,453
r^{2}SCANh	GH (10%)	0,13	0,05	3	0,457
r^{2}SCAN0	GH (25%)	0,21	0,21	1,5	0,462
ωB97X-D3	RSH (20–100%)	0,21	0,42	0,5	0,464

ωB97M-V	RSH (15–100%)	0,21	0,42	0,5	0,465
ωM06-D3	RSH (27–100%)	0,24	0,46	0	0,475
SCAN	L	0,10	0,17	3	0,480
MN15-L	L	0,16	0,05	3	0,483
M06-L	L	0,10	0,17	3	0,486
r^{2}SCAN	L	0,10	0,17	3	0,488
revM11	RSH (23–100%)	0,24	0,45	0,5	0,514
ωB97X-V	RSH (17–100%)	0,23	0,48	0,5	0,518
TPSS	L	0,11	0,29	3	0,554
M11	RSH (43–100%)	0,24	0,44	1	0,563
BP86	L	0,12	0,35	3	0,591
PBE	L	0,12	0,35	3	0,593
BLYP	L	0,12	0,36	3	0,597
TD-HF/RPA	WFT	0,49	0,95	0,5	0,95
CIS	WFT	0,89	1,31	1	1,31

It is found that global-hybrid functionals are the only functionals that provide a balanced description of the whole absorption spectra if the exact exchange is applied in a low to moderate percentage. PW6B95, B3LYP, M06, r^{2}SCANh, and TPSSh universally represent some of the best methods and the latter four have in common that their exact exchange percentage is close to 25%. On the other hand, global hybrids with a high percentage of exact exchange, like MN15 or M08-SO, catch the eye since their wMUE meets the standards of functionals with low to moderate percentage of exact exchange.

One might wonder how decimal numbers are observed for the ghost states and how a decimal number of such a transition can be interpreted. As mentioned before, ghost states refer to over stabilized charge transfer transitions and occur as additional peaks in the spectrum. The probability for these transitions to occur is either one or zero and there is no such thing as one-half (0.5) of a ghost state in an absorption spectrum. These numbers are the result of the average number of GS calculated for the four different transitions (Q- and B-band). We mainly expect GS to occur between the Q- and B-band, rather than inside the bands. Moreover, it is assumed that the HOMO-1 will not show any GS and therefore we only focus on the three remaining states. In conclusion, ghost state(s) might be found for some transition, but not for other transitions, which can result in a decimal number if the average is calculated.

Among all tested range-separated hybrid methods, CAM-B3LYP performed the best with a wMUE of 0.401, while B97M-V yielded a wMUE of 0.453 and therefore stands as the best local one. However, range-separated hybrids tend to overestimate energies of relevant transitions, while local functionals over-stabilize CT ghost states significantly. Therefore, it is advised to use global hybrid functionals with a moderate percentage of exact exchange to model Chl a. It is to be noted, that the addition of the kinetic

energy density does not result in a perceptible change. Furthermore, the use of the rung-2 Generalized Gradient Approximation (GGA) approximation and rung-3 meta-GGA approximation did not exert a substantial influence on the obtained results. In DFT "rung" indicates the level of complexity and accuracy expected for XC functionals, based on the rungs of Jacobs ladder. Jacobs ladder is a hierarchy of XC functionals that increase in accuracy and complexity with each rung. Starting from rung 1 being the LDA, over rung 2 being GGA, mGGA, hybrid functionals, RSH functionals, DH functionals and lastly rung 7 called "beyond-DFT methods", like CC methods or many.body perturbation theory.[160,161]

Now we want to focus on two other features that can influence the accuracy and the cost of TDDFT calculations. Firstly, we investigate a change of symmetry in Chl a. Sirohiwal *et al.* already reported some dependence of the outcome in regards to the molecular geometry by using the complete Chl a molecule with 135 atoms.[55] We followed in their footsteps by extracting the geometry from the crystal structure of photosystem II, afterwards we optimized the data in the gas phase utilizing the GFN2-xtb method, which is implemented in the xtb programme.[162]

Table A1, found in the appendix, shows the geometry of the smallest significantly representative Chl a molecule (in the xyz format) in the gas phase, which was optimized utilizing the CAM-B3LYP-D3(BJ)/def2-TZVP method. The data clearly proves that most trends as well as the general results do not change significantly. We can confirm however that the results depend on the rotation of the vinyl group just as Sirohiwal *et al.* reported.[55] It seems that range-separated hybrid functionals are especially sensitive to this rotation, which was evident in the blue-shift of the Q-band by an average of 0.1 eV and a blue-shift of the B-band by 0.2 eV observed by comparison of the CAM-B3LYP geometry to the full geometry. Moreover, we found that local functionals depend significantly on the geometry. Local functionals over-stabilize various CT states that have a delocalized charge between the phythyl chain and the ring because of their exchange-correlation potential´s incorrect asymptotic behavior. To illustrate this issue further we use popular functionals like PBE and BLYP, which predict three CT states between the Q_x and B_x transitions if the CAM-B3LYP geometry is used. If the full geometry is used CT states between Q_x and B_x are observed and additionally three CT states are found between B_x and B_y. Such a large number of GS complicates the interpretation of spectra significantly and increases the computational cost. Therefore, we generally encourage to stay away from local functionals for the computation of Chl absorption spectra. Instead, it is advised to use global hybrid functionals with a moderate percentage of exact exchange, since they are less affected by geometry changes and show the best compromise between cost and accuracy.

Lastly, we investigate the Tamm-Dancoff approximation (section 2.2.3), which essentially neglects the deexcitation amplitudes in the time-dependent density functional theory eigenvalue problem. The results are shown in Table A2, found in the appendix. However, the results obtained using Tamm-Dancoff differ from the full TDDFT results. One can conclude that excited states are sensitive to correlation effects, which are not sufficiently described by the Tamm-Dancoff approximation.

3.1.2 TDDFT calculations for Phot0 absorption spectra

Another part of this thesis takes a closer look at the molecule phot0 (structure shown in Figure 10), which was first described by de la Concepcion *et al*.[58] As explained in the Introduction phot0 is believed to be a potential precursor for photopigments like chlorophylls, which is why we chose to analyze this molecule. De la Concepción *et al.* computed the absorption spectrum of phot0 with zinc Zn^{2+} and the standard magnesium Mg^{2+} metal centers. Exploring the effect of metal centers on the peak shift is interesting, since exoplanets might have different compositions and other elements are more abundant. On Earth photopigments contain only magnesium as metal center, but show a variety of side chains that influence the peak position. This work explores the peak shift in the absorption spectra of the phot0 structure based on electronegativities of metal and introduces a new structure of phot0 with a calcium Ca^{2+} metal center. Calcium was selected since its properties align with the other metals (magnesium and zinc) as it has a similar size and charge. One property that mainly distinguishes the metals is their electronegativity. Magnesium shows an electronegativity of $\chi_{Mg} = 1.2$, zinc has an EN of $\chi_{Zn} = 1.5$, and lastly, calcium shows an EN of about $\chi_{Ca} = 1.0$.[163] Magnesium (phot0-Mn) serves as the benchmark since it occurs in chlorophylls on Earth and phot0-Zn and phot0-Ca are compared with its absorption spectrum.

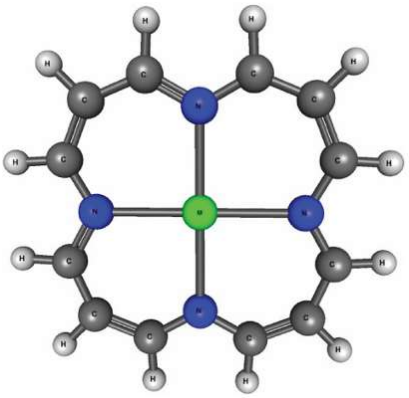

Figure 10: Structure of phot0 with metal center M build using IQmol. Zink (phot0-Zn), calcium (phot0-Ca), and magnesium (phot0-Mg) can take the place of M in this structure.

Employing the DLPNO-STEOM-CCSD method benchmark spectra calculations for all molecules in the gas phase were performed. The geometry was always optimized at the CAM-B3LYP-D3(BJ)/def-TZVP level. The calculations were performed with ORCA 5.0.4 with analogous settings to the ones described in Sirohiwal et al. for Chl a.[55,164] The complete results and detailed data can be found in the appendix (tables A3 to A10). It is important to note that all molecules have a closed shell singlet ground state. The results are summarized in Table 3 below and their spectra are visualized in Figure 11.

Judging by the results, the hypothesis that changing the metal center modulates the absorption maxima for the Q- and B-band is validated. The observed shifts are consistent with the initial thought that metals can conjugate their p orbital with the π electrons in the HOMO of the ring structure. More specifically the a_{2u} symmetric orbital in phot0 can interact with an orbital of a_2 symmetry.

Table 3: VEEs (in eV) associated with the Soret- and Q-bands of different phot0 molecules (phot0-Mg, phot0-Zn, phot0-Ca) calculated with the DLPNO-STEOM-CCSD method and B3LYP-D3(BJ)/def2-TZVP optimized geometries.[40]

	Q_y			**Q_x**		
Metallic center:	**Energy (eV)**	**Wavelength (nm)**	**Oscillator Strength (arbitrary units)**	**Energy (eV)**	**Wavelength (nm)**	**Oscillator Strength (arbitrary units)**
Ca	2.141 (1)	579	0.063	2.141 (2)	579	0.064
Mg	2.165 (1)	574	0.112	2.166 (2)	574	0.112
Zn	2.210 (1)	561	0.127	2.214 (2)	560	0.127
	B_x			**B_y**		
	Energy (eV)	**Wavelength (nm)**	**Oscillator Strength (arbitrary units)**	**Energy (eV)**	**Wavelength (nm)**	**Oscillator Strength (arbitrary units)**
Ca	3.770 (5)	329	1.205	3.775 (6)	329	1.204
Mg	3.900 (4)	318	1.046	3.900 (5)	318	1.046
Zn	3.985 (4)	311	1.019	3.986 (5)	311	1.013

Gouterman hypothesized that an increase in electronegativity of the metal results in a lowered HOMO → LUMO energy and a simultaneous increase of the HOMO-1 → LUMO+1 energy.[41,165] As a consequence the Q-band shows more HOMO → LUMO character as Q_y band is composed of 0.80/0.20 in phot0-Ca, has a ratio of 0.86/0.14 in phot0-Mg, and increases to 0.88/0.12 in phot0-Zn. These changes result in a blue shift in the absorption Q-band, which is also known as a hypsochromic effect. On the other hand, the B_y band experiences a redshift (bathochromic effect) when a more electronegative metal is employed since the B_y state gains more HOMO-1 → LUMO+1 character. This hypophysis was validated by our results, which clearly show a red shifted signal for phot0-Ca and a blue-shifted peak for phot0-Zn, as seen from the inset of Figure 11 depicting the B-band spectra for the three different choices of metals.

The intensities of the Q- and B-bands were calculated using the transition dipole moments and show that the Q-band increases in intensity and the B-band decreases in intensity with electronegativity. The increase and decrease of the bands can be described by the hyperchromic and hypochromic effects.[40] The hyperchromic effect is referring to the increased intensity observed for absorption maxima, while the hypochromic effect yields in an intensity decrease due to geometry distortion of some sort.[166]

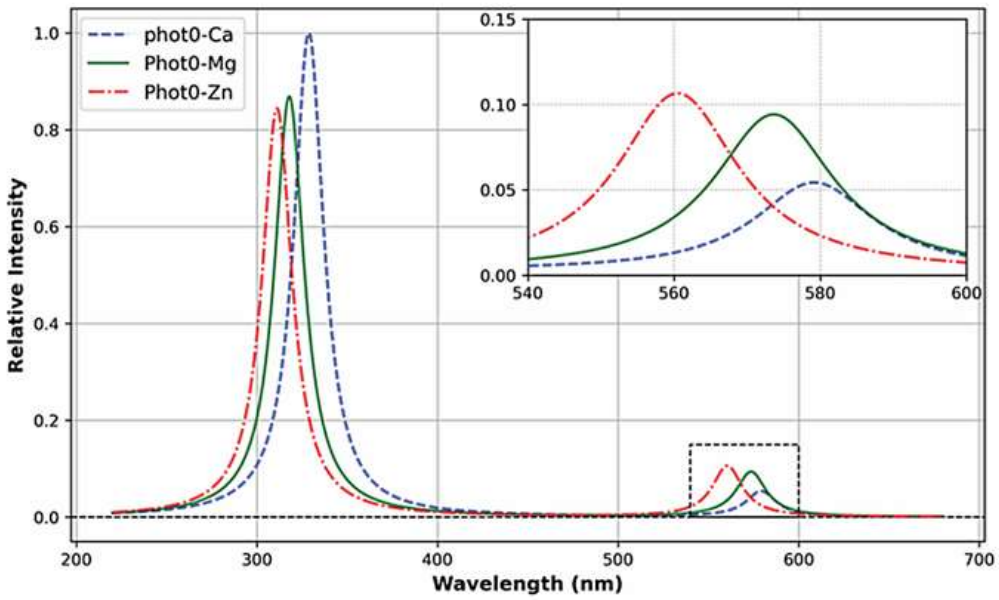

Figure 11: Simulated UV/Vis- absorption spectra for phot0 molecules with different metal centers (phot0-Ca in blue, phot0-Zn in red, and phot0-Mg in green). The peak intensities were calculated with the DLPNO-STEOM-CCSD method and broadened using Lorentzian broadening (broadening parameter $\gamma = 10$).[40]

We moreover used phot0 to further validate our previously established TDDFT results by calculating all three phot0 molecules with the entirety of the exchange-correlation functionals mentioned in the previous section about Chl a. All calculations were carried out using Q-Chem 6.1, except for the B2PLYP and ωB2PLYP calculations, which were performed using ORCA 5.0.4. The results were analyzed under the same aspects established for Chl a (Q-MUE, B-MUE, #GS, and wMUE) and are reported in Table 4. The detailed data is reported in the appendix (tables A5 to A8). From the results, it is clear that the Q-band is accurately described, whereas the B-band generally meets the DLPNO-STEOM-CCSD benchmark, except for calculations with local functionals. Phot0 molecules seem to be able to employ a larger percentage of exact exchange, ranging from 20-50%. In agreement with the chlorophyll results, PW6B95 and M06 functionals perform well. Additionally, Minnesota functionals, like the M06-2X, MN15, and also M08-SO functional yield good results, while range-separated functionals produce underwhelming results.

Table 4: Overview of all the tested methods and their mean unassigned errors (MUEs) for phot0. The errors were calculated with respect to the DLPNO-STEOM-CCSD benchmark. Three statistical indicators were used to calculate the weighted MUE (wMUE): MUE for the peak positions of the Q-band; B-MUE: MUE for the peak positions of the B-band; #GS: average number of 'ghost states' between the Q- and B-band. The color scheme indicated the performance with decreasing accuracy from green (best) to red (worst).[40] Labels for the functional type are equivalent to the labels found in Table 1.

Method:	Type	Q-MUE	B-MUE	#GS	wMUE
B2PLYP	DH	0,06	0,27	0,33	0,231
PW6B95	GH (28%)	0,18	0,06	0,00	0,206
ωB2PLYP	RS-DH	0,05	0,14	0,33	0,153
M06	GH (27%)	0,03	0,19	0,00	0,121
B3LYP	GH (20%)	0,04	0,19	0,67	0,201
MN15	GH (44%)	0,02	0,11	0,33	0,108
M08-SO	GH (57%)	0,05	0,10	0,00	0,106
CAM-B3LYP	RSH (19–100%)	0,07	0,08	0,33	0,146
PBE0	GH (25%)	0,07	0,11	0,33	0,160
LC-ωPBEh	RSH (20–100%)	0,08	0,08	0,67	0,180
ωB97X-D	RSH (17–100%)	0,10	0,08	0,67	0,204
LC-ωPBE	RSH (0–100%)	0,14	0,07	1,00	0,276
TPSSh	GH (10%)	0,08	0,18	0,67	0,233
M06-2X	GH (54%)	0,02	0,08	0,33	0,089

M08-HX	GH (52%)	0,07	0,08	0,67	0,173
ωM05-D	RSH (37–100%)	0,10	0,07	1,33	0,268
B97M-V	L	0,06	0,17	0,67	0,209
r2SCANh	GH (10%)	0,12	0,09	0,67	0,228
r2SCAN0	GH (25%)	0,11	0,08	0,33	0,183
ωB97X-D3	RSH (20–100%)	0,17	0,09	0,67	0,283
ωB97M-V	RSH (15–100%)	0,24	0,09	0,33	0,317
ωM06-D3	RSH (27–100%)	0,20	0,10	1,67	0,417
SCAN	L	0,02	0,15	0,33	0,130
MN15-L	L	0,14	0,08	0,33	0,214
M06-L	L	0,09	0,16	1,00	0,270
r2SCAN	L	0,10	0,16	0,67	0,246
revM11	RSH (23–100%)	0,34	0,08	0,67	0,445
ωB97X-V	RSH (17–100%)	0,24	0,10	0,67	0,359
TPSS	L	0,02	0,25	1,33	0,276
M11	RSH (43–100%)	0,14	0,08	0,33	0,218
BP86	L	0,02	0,35	0,67	0,261
PBE	L	0,02	0,35	0,33	0,229
BLYP	L	0,02	0,39	0,33	0,245

Chapter 4

4.1 Conclusion

The evolution of oxygenic photosynthesis is commonly recognized as a significant event in Earth's evolutionary history, potentially providing implications for extraterrestrial life on exoplanets. Up until today no extraterrestrial life has been found and the search continues. For the development of new telescopes, a deeper understanding of absorption spectra is beneficial. On Earth, chlorophylls are the primary photopigments in photosynthesis and play a vital role in astrobiology by generating the vegetation red edge biosignature. In the search for extraterrestrial life biosignatures like the VRE are important. The VRE specifically is a robust biosignature, meaning that no false negatives or false positives are known.[15,29] Observation of such a signal can therefore indicate the existence of life. However, as described in section 1.2, many scientists have made the point that other star systems can have different peak absorption wavelength, which can lead to the evolution of different photopigments or derivates of photopigments known on Earth.[18,20–26] If the photopigments have different structures they can absorb light in different regions, yielding in a shifted VRE. Therefore, it is crucial to accurately model photopigments, especially the Q-band, to determine where the VRE would occur. Surprisingly, despite the widely acknowledged significance of photosynthesis and photopigments, there exists only a limited amount of studies modeling their structures and absorption spectra from a computational chemistry perspective.

To address this gap, this work focuses on benchmarking time-dependent density-functional theory absorption spectra of photopigments like Chl a. We can conclude that among all 25 tested methods Chl a is best described by the B2PLYP double-hybrid functional and PW6B95 global-hybrid functional. The original intention to find a TDDFT functional with comparable accuracy to B2PLYP was therefore met. Moreover, did the results clearly indicate that local functionals show a tendency to over-stabilize CT ghost-states, while range-separated functionals yielded red-shifted energy states. The optimal compromise between accuracy and computational cost is met by implementing global hybrid functionals with a moderate percentage of exact exchange.

Additionally, the study investigates the absorption spectrum of the potential photopigment precursor "phot0". In analogy to the benchmark calculations for Chla, the peak positions of the Q- and B-bands for phot0 were calculated using the same functionals. The results agree with Chl a that local functionals should be avoided. Global-hybrid functionals performed the best overall and the MN15, M08-SO, and M06-2X functionals showed the highest accuracies. Lastly, different central metal ions (Mg, Ca, or Zn)

in phot0 were analyzed. By using the DLPNO-STEOM-CCSD method, the effect of the electronegativity of the metal ion on absorption spectra was explored. The results validate the Gouterman hypothesis and indicate that a spectral shift directly correlated with the central metal electronegativity. For example, a blue-shift is caused by more electronegative metals and vice versa.

4.2 Outlook

This work serves as a preliminary study for the prediction of absorption spectra of photopigments like chlorophyll a (Chl a). However, further research is needed to optimize the performance of the computational methods for the modeling of the absorption spectra. Further investigation of the vibronic structure in absorption spectra is especially important since these effects were implicitly absent in this work. Additionally, it is important to investigate environmental effects on the peak shift, that occurs for example at different temperatures or is caused by solvent effects.

Moreover, this work focused purely on absorption and absorption spectra, and other spectral properties were not a concern. However, Chl a fluorescence induction has been used widely as a probe to study photosynthesis and has been proposed in the literature as a biosignature.[15,15] If an excited molecule relaxes into a lower energy state over the emission of a photon and simultaneously remains in the existing spin state, one observes fluorescence. Illuminating dark-adapted leaves gives rise to fluorescence from the photo system II, PSII, which is described by the Kautsky effect.[167] Therefore it could be of interest to forecast fluorescence and phosphorescence rates.

Future research should involve more photopigments, instead of just Chl a and phot0. Our work revolves mainly around Chl a and its potential precursor phot0, however, there is a variety of photopigments we have not analyzed, yet. While Chl a is one of the most, if not the most important, chlorophyll on Earth, there is no guarantee that it will be the most important photopigment on exoplanets. The results found for Chl a need to be validated for other porphyrin structures as well. A good candidate is Chlorophyll b (Chl b), since it occurs in a variety of organisms that undergo photosynthesis and is important for photosynthesis on Earth. Aside from other chlorophylls the absorption spectra of bacteriochlorophylls, carotenoids, or cyanophycin should be explored as well.

With this work three different metal centers were tested in phot0, however many others can be analyzed as well. Iron seems to be the obvious choice, since it occurs in haemoglobine and is generally an abundant element in the Universe. This work only used metals that are in the singlet state, but the research should explore more metals to further validate Gouterman´s hypothysis. This work does not

tackle how the electronegativity of the metal influences the orbital energies of the frontier orbitals. This could be explored in future works.

Lastly, it is important to determine the effect different metal centers have on the multiple facets of photosynthetic activity such as electronic excitation. It is unclear how and if different metal centers, or absence of metal centers, will influence the photosynthetic activity.

In conclusion, this thesis serves as a preliminary study and highlights the importance of accurately modelling absorption spectra of photopigments via DFT with a specific focus on lowering the computational cost. In the past, wave function theory methods have dominated the computational modelling of photopigments like chlorophyll a, however DFT provides an alternative approach. In the search of life photosynthesis and photopigments have been investigated and many research groups hypothesize how extraterrestrial photopigments could look like. With the development of new empirical and theoretical methods, it becomes more and more important to accurately model such molecules. This knowledge, has the potential to facilitate their detection using future telescopes (ground- or space-based). However, at the moment, the modelled spectra are simplified and require the inclusion of other factors, such as understanding and implementing the vibronic structure, and considering the impact of environmental effects (temperature variations, solvent effects, …). By addressing these factors, we aim to deepen our understanding of absorption characteristics of terrestrial and potential extraterrestrial photopigments, and perhaps pave the way for their detection in the future. A successful detection could greatly further our knowledge of the rarity or commonality of life in the Universe.[168]

References

(1) Schönegger, V. Altgriechisches Herkunftswörterbuch. **2007**.
(2) Rabinowitch, E. I.; Govindjee. The Role of Chlorophyll in Photosynthesis. *Sci. Am.* **1965**, *213* (1), 74–83. https://doi.org/10.1038/scientificamerican0765-74.
(3) Bar-On, Y. M.; Phillips, R.; Milo, R. The Biomass Distribution on Earth. *Proc. Natl. Acad. Sci.* **2018**, *115* (25), 6506–6511. https://doi.org/10.1073/pnas.1711842115.
(4) Field, C. B.; Behrenfeld, M. J.; Randerson, J. T.; Falkowski, P. Primary Production of the Biosphere: Integrating Terrestrial and Oceanic Components. *Science* **1998**, *281* (5374), 237–240. https://doi.org/10.1126/science.281.5374.237.
(5) Lindeman, R. L. The Trophic-Dynamic Aspect of Ecology. **2024**.
(6) Frankelius, P. A Proposal to Rethink Agriculture in the Climate Calculations. *Agron. J.* **2020**, *112* (4), 3216–3221. https://doi.org/10.1002/agj2.20286.
(7) Emerson, R.; Arnold, W. THE PHOTOCHEMICAL REACTION IN PHOTOSYNTHESIS. . *J. Gen. Physiol* **1932**, No. 16, 191–205.
(8) Renger, G. The Light Reactions of Photosynthesis. *Curr. Sci.* **2010**, *98* (10).
(9) Pearlstein, R. M. Chlorophyll Singlet Exciton. In *Photosynthesis 1, Energy Conversion by Plants and Bacteria*; Academic Press: New York, UNITED STATES, 1982.
(10) Buchner, T. B.; Ewingen, N. H. *Photosynthesis: Theory and Applications in Energy, Biotechnology and Nanotechnology*; Nova Science Publishers, Incorporated: New York, UNITED STATES, 2009.
(11) Blankenship, R. E. Early Evolution of Photosynthesis. *Plant Physiol.* **2010**, *154* (2), 434–438. https://doi.org/10.1104/pp.110.161687.
(12) Hamilton, T. L. The Trouble with Oxygen: The Ecophysiology of Extant Phototrophs and Implications for the Evolution of Oxygenic Photosynthesis. *Free Radic. Biol. Med.* **2019**, *140*, 233–249. https://doi.org/10.1016/j.freeradbiomed.2019.05.003.
(13) Buick, R. When Did Oxygenic Photosynthesis Evolve? *Philos. Trans. R. Soc. B Biol. Sci.* **2008**, *363* (1504), 2731–2743. https://doi.org/10.1098/rstb.2008.0041.
(14) Olson, J. M. Photosynthesis in the Archean Era. *Photosynth. Res.* **2006**, *88* (2), 109–117. https://doi.org/10.1007/s11120-006-9040-5.
(15) Lingam, M.; Loeb, A. *Life in the Cosmos*; Harvard University Press, 2021.
(16) Perry, J. In What Part of the Electromagnetic Spectrum Does the Sun Emit Energy? **2022**.
(17) Björn, L. O.; Papageorgiou, G. C.; Blankenship, R. E.; Govindjee. A Viewpoint: Why Chlorophyll a? *Photosynth. Res.* **2009**, *99* (2), 85–98. https://doi.org/10.1007/s11120-008-9395-x.
(18) Lehmer, O. R.; Catling, D. C.; Parenteau, M. N.; Kiang, N. Y.; Hoehler, T. M. The Peak Absorbance Wavelength of Photosynthetic Pigments Around Other Stars From Spectral Optimization. *Front. Astron. Space Sci.* **2021**, *8*, 689441. https://doi.org/10.3389/fspas.2021.689441.
(19) Marosvölgyi, M. A.; van Gorkom, H. J. Cost and Color of Photosynthesis. *Photosynth. Res.* **2010**, *103* (2), 105–109. https://doi.org/10.1007/s11120-009-9522-3.
(20) Wolstencroft, R. D.; Raven, J. A. Photosynthesis: Likelihood of Occurrence and Possibility of Detection on Earth-like Planets. *Icarus* **2002**, *157* (2), 535–548. https://doi.org/10.1006/icar.2002.6854.

(21) Kiang, N. Y.; Segura, A.; Tinetti, G.; Govindjee; Blankenship, R. E.; Cohen, M.; Siefert, J.; Crisp, D.; Meadows, V. S. Spectral Signatures of Photosynthesis. II. Coevolution with Other Stars And The Atmosphere on Extrasolar Worlds. *Astrobiology* **2007**, *7* (1), 252–274. https://doi.org/10.1089/ast.2006.0108.
(22) Duffy, C. D. P.; Canchon, G.; Haworth, T. J.; Gillen, E.; Chitnavis, S.; Mullineaux, C. W. Photosynthesis under a Red Sun: Predicting the Absorption Characteristics of an Extraterrestrial Light-Harvesting Antenna. *Mon. Not. R. Astron. Soc.* **2023**, *526* (2), 2265–2277. https://doi.org/10.1093/mnras/stad2823.
(23) Lingam, M.; Balbi, A.; Mahajan, S. M. Excitation Properties of Photopigments and Their Possible Dependence on the Host Star. *Astrophys. J. Lett.* **2021**, *921* (2), L41. https://doi.org/10.3847/2041-8213/ac3478.
(24) Lingam, M.; Ginsburg, I.; Loeb, A. Prospects for Life on Temperate Planets around Brown Dwarfs. *Astrophys. J.* **2020**, *888* (2), 102. https://doi.org/10.3847/1538-4357/ab5b13.
(25) Lingam, M.; Loeb, A. Brown Dwarf Atmospheres as the Potentially Most Detectable and Abundant Sites for Life. *Astrophys. J.* **2019**, *883* (2), 143. https://doi.org/10.3847/1538-4357/ab3f35.
(26) Lingam, M.; Loeb, A. Photosynthesis on Exoplanets and Exomoons from Reflected Light. *Int. J. Astrobiol.* **2020**, *19* (3), 210–219. https://doi.org/10.1017/S1473550419000247.
(27) Marais, D. J. D.; Allamandola, L. J.; Benner, S. A.; Boss, A. P.; Deamer, D.; Falkowski, P. G.; Farmer, J. D.; Hedges, S. B.; Jakosky, B. M.; Knoll, A. H.; Liskowsky, D. R.; Meadows, V. S.; Meyer, M. A.; Pilcher, C. B.; Nealson, K. H.; Spormann, A. M.; Trent, J. D.; Turner, W. W.; Woolf, N. J.; Yorke, H. W. The NASA Astrobiology Roadmap.
(28) Des Marais, D. J.; Nuth, J. A.; Allamandola, L. J.; Boss, A. P.; Farmer, J. D.; Hoehler, T. M.; Jakosky, B. M.; Meadows, V. S.; Pohorille, A.; Runnegar, B.; Spormann, A. M. The NASA Astrobiology Roadmap. *Astrobiology* **2008**, *8* (4), 715–730. https://doi.org/10.1089/ast.2008.0819.
(29) Schwieterman, E. W.; Kiang, N. Y.; Parenteau, M. N.; Harman, C. E.; DasSarma, S.; Fisher, T. M.; Arney, G. N.; Hartnett, H. E.; Reinhard, C. T.; Olson, S. L.; Meadows, V. S.; Cockell, C. S.; Walker, S. I.; Grenfell, J. L.; Hegde, S.; Rugheimer, S.; Hu, R.; Lyons, T. W. Exoplanet Biosignatures: A Review of Remotely Detectable Signs of Life. *Astrobiology* **2018**, *18* (6), 663–708. https://doi.org/10.1089/ast.2017.1729.
(30) Seager, S.; Schrenk, M.; Bains, W. An Astrophysical View of Earth-Based Metabolic Biosignature Gases. *Astrobiology* **2012**, *12* (1), 61–82. https://doi.org/10.1089/ast.2010.0489.
(31) Meadows, V. S. Reflections on O_2 as a Biosignature in Exoplanetary Atmospheres. *Astrobiology* **2017**, *17* (10), 1022–1052. https://doi.org/10.1089/ast.2016.1578.
(32) Meadows, V. S.; Reinhard, C. T.; Arney, G. N.; Parenteau, M. N.; Schwieterman, E. W.; Domagal-Goldman, S. D.; Lincowski, A. P.; Stapelfeldt, K. R.; Rauer, H.; DasSarma, S.; Hegde, S.; Narita, N.; Deitrick, R.; Lustig-Yaeger, J.; Lyons, T. W.; Siegler, N.; Grenfell, J. L. Exoplanet Biosignatures: Understanding Oxygen as a Biosignature in the Context of Its Environment. *Astrobiology* **2018**, *18* (6), 630–662. https://doi.org/10.1089/ast.2017.1727.
(33) Committee on Astrobiology Science Strategy for the Search for Life in the Universe; Space Studies Board; Division on Engineering and Physical Sciences; National Academies of Sciences, Engineering, and Medicine. *An Astrobiology Strategy for the*

Search for Life in the Universe; National Academies Press: Washington, D.C., 2019; p 25252. https://doi.org/10.17226/25252.
(34) Dorn, E. D.; Adami, C. Robust Monomer-Distribution Biosignatures in Evolving Digital Biota. *Astrobiology* **2011**, *11* (10), 959–968. https://doi.org/10.1089/ast.2010.0556.
(35) Catling, D. C.; Krissansen-Totton, J.; Kiang, N. Y.; Crisp, D.; Robinson, T. D.; DasSarma, S.; Rushby, A. J.; Del Genio, A.; Bains, W.; Domagal-Goldman, S. Exoplanet Biosignatures: A Framework for Their Assessment. *Astrobiology* **2018**, *18* (6), 709–738. https://doi.org/10.1089/ast.2017.1737.
(36) Gebauer, S.; Grenfell, J. L.; Stock, J. W.; Lehmann, R.; Godolt, M.; Von Paris, P.; Rauer, H. Evolution of Earth-like Extrasolar Planetary Atmospheres: Assessing the Atmospheres and Biospheres of Early Earth Analog Planets with a Coupled Atmosphere Biogeochemical Model. *Astrobiology* **2017**, *17* (1), 27–54. https://doi.org/10.1089/ast.2015.1384.
(37) Knoll, A. H. *Life on a Young Planet*; Princeton University Press, 2015.
(38) Neveu, M.; Hays, L. E.; Voytek, M. A.; New, M. H.; Schulte, M. D. The Ladder of Life Detection. *Astrobiology* **2018**, *18* (11), 1375–1402. https://doi.org/10.1089/ast.2017.1773.
(39) *Chlorophylls and Bacteriochlorophylls: Biochemistry, Biophysics, Functions and Applications*; Grimm, B., Ed.; Advances in photosynthesis and respiration; Springer: Dordrecht, 2006.
(40) Illner, D.; Lingam, M.; Peverati, R. On the Importance and Challenges of Modelling Extraterrestrial Photopigments via Density-Functional Theory. *Mol. Phys.* **2023**, e2261563. https://doi.org/10.1080/00268976.2023.2261563.
(41) Gouterman, M. Spectra of Porphyrins. *J. Mol. Spectrosc.* **1961**, *6*, 138–163.
(42) Gruber, E.; Kjær, C.; Nielsen, S. B.; Andersen, L. H. Intrinsic Photophysics of Light-harvesting Charge-tagged Chlorophyll *a* and *b* Pigments. *Chem. – Eur. J.* **2019**, *25* (39), 9153–9158. https://doi.org/10.1002/chem.201901786.
(43) Hasegawa, J.; Ozeki, Y.; Ohkawa, K.; Hada, M.; Nakatsuji, H. Theoretical Study of the Excited States of Chlorin, Bacteriochlorin, Pheophytin *a* , and Chlorophyll *a* by the SAC/SAC−CI Method. *J. Phys. Chem. B* **1998**, *102* (7), 1320–1326. https://doi.org/10.1021/jp972894o.
(44) Sundholm, D. Density Functional Theory Calculations of the Visible Spectrum of Chlorophyll a. *Chem. Phys. Lett.* **1999**, *302* (5–6), 480–484. https://doi.org/10.1016/S0009-2614(99)00194-3.
(45) Sundholm, D. Comparison of the Electronic Excitation Spectra of Chlorophyll a and Pheophytin a Calculated at Density Functional Theory Level. *Chem. Phys. Lett.* **2000**, *317* (6), 545–552. https://doi.org/10.1016/S0009-2614(99)01428-1.
(46) Parusel, A. B. J.; Grimme, S. A Theoretical Study of the Excited States of Chlorophyll *a* and Pheophytin *a*. *J. Phys. Chem. B* **2000**, *104* (22), 5395–5398. https://doi.org/10.1021/jp000346w.
(47) Cai, Z.-L.; Crossley, M. J.; Reimers, J. R.; Kobayashi, R.; Amos, R. D. Density Functional Theory for Charge Transfer: The Nature of the N-Bands of Porphyrins and Chlorophylls Revealed through CAM-B3LYP, CASPT2, and SAC-CI Calculations. *J. Phys. Chem. B* **2006**, *110* (31), 15624–15632. https://doi.org/10.1021/jp063376t.

(48) Cai, Z.-L.; Sendt, K.; Reimers, J. R. Failure of Density-Functional Theory and Time-Dependent Density-Functional Theory for Large Extended π Systems. *J. Chem. Phys.* **2002**, *117* (12), 5543–5549. https://doi.org/10.1063/1.1501131.
(49) Dahlbom, M. G.; Reimers *, J. R. Successes and Failures of Time-Dependent Density Functional Theory for the Low-Lying Excited States of Chlorophylls. *Mol. Phys.* **2005**, *103* (6–8), 1057–1065. https://doi.org/10.1080/00268970412331333528.
(50) Reimers, J. R.; Cai, Z.-L.; Kobayashi, R.; Rätsep, M.; Freiberg, A.; Krausz, E. Assignment of the Q-Bands of the Chlorophylls: Coherence Loss via Qx − Qy Mixing. *Sci. Rep.* **2013**, *3* (1), 2761. https://doi.org/10.1038/srep02761.
(51) Heimdal, J.; Jensen, K. P.; Devarajan, A.; Ryde, U. The Role of Axial Ligands for the Structure and Function of Chlorophylls. *JBIC J. Biol. Inorg. Chem.* **2006**, *12* (1), 49–61. https://doi.org/10.1007/s00775-006-0164-z.
(52) Milne, B. F.; Toker, Y.; Rubio, A.; Nielsen, S. B. Unraveling the Intrinsic Color of Chlorophyll. *Angew. Chem. Int. Ed.* **2015**, *54* (7), 2170–2173. https://doi.org/10.1002/anie.201410899.
(53) Stockett, M. H.; Musbat, L.; Kj, C.; Rubio, A.; Milne, B. F.; Nielsen, S. B. The Soret Absorption Band of Isolated Chlorophyll a and b Tagged with Quarternary Ammonium Ions. **2012**.
(54) Wellman, S. M. J.; Jockusch, R. A. Moving in on the Action: An Experimental Comparison of Fluorescence Excitation and Photodissociation Action Spectroscopy. *J. Phys. Chem. A* **2015**, *119* (24), 6333–6338. https://doi.org/10.1021/acs.jpca.5b04835.
(55) Sirohiwal, A.; Berraud-Pache, R.; Neese, F.; Izsák, R.; Pantazis, D. A. Accurate Computation of the Absorption Spectrum of Chlorophyll *a* with Pair Natural Orbital Coupled Cluster Methods. *J. Phys. Chem. B* **2020**, *124* (40), 8761–8771. https://doi.org/10.1021/acs.jpcb.0c05761.
(56) Bai, S.; Mansour, R.; Stojanović, L.; Toldo, J. M.; Barbatti, M. On the Origin of the Shift between Vertical Excitation and Band Maximum in Molecular Photoabsorption. *J. Mol. Model.* **2020**, *26* (5), 107. https://doi.org/10.1007/s00894-020-04355-y.
(57) Diehl, R.; Korn, A. J.; Leibundgut, B.; Lugaro, M.; Wallner, A. Cosmic Nucleosynthesis: A Multi-Messenger Challenge. *Prog. Part. Nucl. Phys.* **2022**, *127*, 103983. https://doi.org/10.1016/j.ppnp.2022.103983.
(58) de la Concepción, J. G.; Cerdán, L.; Marcos-Arenal, P.; Burillo-Villalobos, M.; Fonseca-Bonilla, N.; Lizcano-Vaquero, R.; López-Cayuela, M.-Á.; Caballero, J. A.; Gómez, F. Phot0, a Plausible Primeval Pigment on Earth and Rocky Exoplanets. *Phys. Chem. Chem. Phys.* **2022**, *24* (28), 16979–16987. https://doi.org/10.1039/D2CP01703B.
(59) Baiardi, A.; Bloino, J.; Barone, V. General Time Dependent Approach to Vibronic Spectroscopy Including Franck–Condon, Herzberg–Teller, and Duschinsky Effects. *J. Chem. Theory Comput.* **2013**, *9* (9), 4097–4115. https://doi.org/10.1021/ct400450k.
(60) Franck, J.; Dymond, E. G. Elementary Processes of Photochemical Reactions. *Trans. Faraday Soc.* **1926**, *21* (February), 536. https://doi.org/10.1039/tf9262100536.
(61) Herzberg, G.; Teller, E. Schwingungsstruktur der Elektronenübergänge bei mehratomigen Molekülen. *Z. Für Phys. Chem.* **1933**, *21B* (1), 410–446. https://doi.org/10.1515/zpch-1933-2136.
(62) Condon, E. U. Nuclear Motions Associated with Electron Transitions in Diatomic Molecules. *Phys. Rev.* **1928**, *32* (6), 858–872. https://doi.org/10.1103/PhysRev.32.858.

(63) Jain, A.; Blum, C.; Subramaniam, V. Fluorescence Lifetime Spectroscopy and Imaging of Visible Fluorescent Proteins. In *Advances in Biomedical Engineering*; Elsevier, 2009; pp 147–176. https://doi.org/10.1016/B978-0-444-53075-2.00004-6.
(64) Dierksen, M.; Grimme, S. Density Functional Calculations of the Vibronic Structure of Electronic Absorption Spectra. *J. Chem. Phys.* **2004**, *120* (8), 3544–3554. https://doi.org/10.1063/1.1642595.
(65) Gupta, V. P. Interaction of Radiation and Matter and Electronic Spectra. In *Principles and Applications of Quantum Chemistry*; Elsevier, 2016; pp 291–337. https://doi.org/10.1016/B978-0-12-803478-1.00009-1.
(66) Avila Ferrer, F. J.; Cerezo, J.; Soto, J.; Improta, R.; Santoro, F. First-Principle Computation of Absorption and Fluorescence Spectra in Solution Accounting for Vibronic Structure, Temperature Effects and Solvent Inhomogenous Broadening. *Comput. Theor. Chem.* **2014**, *1040–1041*, 328–337. https://doi.org/10.1016/j.comptc.2014.03.003.
(67) Parr, R. G.; Yang, W. *Density-functional Theory of Atoms and Molecules*; Oxford University Press, 1989; Vol. 47.
(68) Zener, C.; Heikes, R. R. Exchange Interactions. *Rev. Mod. Phys.* **1953**, *25* (1), 191–198. https://doi.org/10.1103/RevModPhys.25.191.2.
(69) Dirac, P. A. M. Note on Exchange Phenomena in the Thomas Atom. *Math. Proc. Camb. Philos. Soc.* **1930**, *26* (3), 376–385. https://doi.org/10.1017/S0305004100016108.
(70) Cramer, C. J. *Essentials of Computational Chemistry: Theories and Models, 2nd Edition*, 2nd ed.; Wiley.
(71) Kohn, W.; Sham, L. J. Self-Consistent Equations Including Exchange and Correlation Effects. *Phys. Rev.* **1965**, *140* (4A), A1133–A1138. https://doi.org/10.1103/PhysRev.140.A1133.
(72) Pople, J. A.; Gill, P. M. W.; Johnson, B. G. Kohn—Sham Density-Functional Theory within a Finite Basis Set. *Chem. Phys. Lett.* **1992**, *199* (6), 557–560. https://doi.org/10.1016/0009-2614(92)85009-Y.
(73) Hartree, D. R.; Hartree, W. Self-Consistent Field, with Exchange, for Beryllium. *Royal Society* **1935**, *150* (869).
(74) Slater, J. C. A Simplification of the Hartree-Fock Method. *Phys. Rev.* **1951**, *81* (3), 385–390. https://doi.org/10.1103/PhysRev.81.385.
(75) Sahni, V. The Hohenberg-Kohn Theorems and Kohn-Sham Density Functional Theory. In *Quantal Density Functional Theory*; Sahni, V., Ed.; Springer: Berlin, Heidelberg, 2004; pp 99–123. https://doi.org/10.1007/978-3-662-09624-6_4.
(76) Ceperley, D. M.; Alder, B. J. Ground State of the Electron Gas by a Stochastic Method. *Phys. Rev. Lett.* **1980**, *45* (7), 566–569. https://doi.org/10.1103/PhysRevLett.45.566.
(77) Liu, K. L.; Vosko, S. H. A Time-Dependent Spin Density Functional Theory for the Dynamical Spin Susceptibility. *Can. J. Phys.* **1989**, *67* (11), 1015–1021. https://doi.org/10.1139/p89-178.
(78) Amusia, M. Y.; Msezane, A. Z.; Shaginyan, V. R. Density Functional Theory versus the Hartree–Fock Method: Comparative Assessment. *Phys. Scr.* **2003**, *68* (6), C133–C140. https://doi.org/10.1238/Physica.Regular.068aC0133.
(79) Marques, M. A. L.; Gross, E. K. U. TIME-DEPENDENT DENSITY FUNCTIONAL THEORY. *Annu. Rev. Phys. Chem.* **2004**, *55* (1), 427–455. https://doi.org/10.1146/annurev.physchem.55.091602.094449.

(80) Becke, A. D. Density-Functional Exchange-Energy Approximation with Correct Asymptotic-Behavior. *Phys. Rev. A* **1988**, *38*, 3098–3100. https://doi.org/10.1103/PhysRevA.38.3098.
(81) Perdew, J. P.; Burke, K.; Ernzerhof, M. Generalized Gradient Approximation Made Simple. *Phys. Rev. Lett.* **1996**, *77*, 3865–3868. https://doi.org/10.1103/PhysRevLett.77.3865.
(82) Peverati, R.; Truhlar, D. G. Quest for a Universal Density Functional: The Accuracy of Density Functionals across a Broad Spectrum of Databases in Chemistry and Physics. *Philos. Trans. R. Soc. Math. Phys. Eng. Sci.* **2014**, *372* (2011), 20120476. https://doi.org/10.1098/rsta.2012.0476.
(83) *Theory and Applications of Satisfiability Testing – SAT 2021: 24th International Conference, Barcelona, Spain, July 5-9, 2021, Proceedings*; Li, C.-M., Manyà, F., Eds.; Lecture Notes in Computer Science; Springer International Publishing: Cham, 2021; Vol. 12831. https://doi.org/10.1007/978-3-030-80223-3.
(84) Perdew, J. P.; Kurth, S.; Zupan, A.; Blaha, P. Accurate Density Functional with Correct Formal Properties: A Step Beyond the Generalized Gradient Approximation. *Phys. Rev. Lett.* **1999**, *82* (12), 2544–2547. https://doi.org/10.1103/PhysRevLett.82.2544.
(85) Atalla, V.; Zhang, I. Y.; Hofmann, O. T.; Ren, X.; Rinke, P.; Scheffler, M. Enforcing the Linear Behavior of the Total Energy with Hybrid Functionals: Implications for Charge Transfer, Interaction Energies, and the Random-Phase Approximation. *Phys. Rev. B* **2016**, *94* (3), 035140. https://doi.org/10.1103/PhysRevB.94.035140.
(86) Foster, R. Electron Donor-Acceptor Complexes. *J. Phys. Chem.* **1980**, *84* (17), 2135–2141. https://doi.org/10.1021/j100454a006.
(87) Dreuw, A.; Head-Gordon, M. Failure of Time-Dependent Density Functional Theory for Long-Range Charge-Transfer Excited States: The Zincbacteriochlorin−Bacteriochlorin and Bacteriochlorophyll−Spheroidene Complexes. *J. Am. Chem. Soc.* **2004**, *126* (12), 4007–4016. https://doi.org/10.1021/ja039556n.
(88) Fabiano, E.; Constantin, L. A.; Cortona, P.; Della Sala, F. Global Hybrids from the Semiclassical Atom Theory Satisfying the Local Density Linear Response. *J. Chem. Theory Comput.* **2015**, *11* (1), 122–131. https://doi.org/10.1021/ct500902p.
(89) Constantin, L. A.; Fabiano, E.; Laricchia, S.; Della Sala, F. Semiclassical Neutral Atom as a Reference System in Density Functional Theory. *Phys. Rev. Lett.* **2011**, *106* (18), 186406. https://doi.org/10.1103/PhysRevLett.106.186406.
(90) Perdew, J. P.; Burke, K.; Ernzerhof, M. Generalized Gradient Approximation Made Simple. *Phys. Rev. Lett.* **1996**, *77* (18), 3865–3868. https://doi.org/10.1103/PhysRevLett.77.3865.
(91) Mardirossian, N.; Head-Gordon, M. Thirty Years of Density Functional Theory in Computational Chemistry: An Overview and Extensive Assessment of 200 Density Functionals. *Mol. Phys.* **2017**, *115* (19), 2315–2372. https://doi.org/10.1080/00268976.2017.1333644.
(92) Mardirossian, N.; Head-Gordon, M. $ømega$B97X-V: A 10-Parameter, Range-Separated Hybrid, Generalized Gradient Approximation Density Functional with Nonlocal Correlation, Designed by a Survival-of-the-Fittest Strategy. *Phys. Chem. Chem. Phys.* **2014**, *16* (21), 9904–9924. https://doi.org/10.1039/c3cp54374a.

(93) Krukau, A. V.; Scuseria, G. E.; Perdew, J. P.; Savin, A. Hybrid Functionals with Local Range Separation. *J. Chem. Phys.* **2008**, *129* (12), 124103. https://doi.org/10.1063/1.2978377.
(94) Mardirossian, N.; Head-Gordon, M. Exploring the Limit of Accuracy for Density Functionals Based on the Generalized Gradient Approximation: Local, Global Hybrid, and Range-Separated Hybrid Functionals with and without Dispersion Corrections. *J. Chem. Phys.* **2014**, *140* (18), 18A527. https://doi.org/10.1063/1.4868117.
(95) Shavitt, I.; Bartlett, R. J. *Many-Body Methods in Chemistry and Physics: MBPT and Coupled-Cluster Theory*, 1st ed.; Cambridge University Press, 2009. https://doi.org/10.1017/CBO9780511596834.
(96) Stanton, J. F.; Bartlett, R. J. The Equation of Motion Coupled-Cluster Method. A Systematic Biorthogonal Approach to Molecular Excitation Energies, Transition Probabilities, and Excited State Properties. *J. Chem. Phys.* **1993**, *98* (9), 7029–7039. https://doi.org/10.1063/1.464746.
(97) Rowe, D. J. Equations-of-Motion Method and the Extended Shell Model. *Rev. Mod. Phys.* **1968**, *40* (1), 153–166. https://doi.org/10.1103/RevModPhys.40.153.
(98) Krylov, A. I. Equation-of-Motion Coupled-Cluster Methods for Open-Shell and Electronically Excited Species: The Hitchhiker's Guide to Fock Space. *Annu. Rev. Phys. Chem.* **2008**, *59* (1), 433–462. https://doi.org/10.1146/annurev.physchem.59.032607.093602.
(99) Nooijen, M.; Bartlett, R. J. Equation of Motion Coupled Cluster Method for Electron Attachment. *J. Chem. Phys.* **1995**, *102* (9), 3629–3647. https://doi.org/10.1063/1.468592.
(100) Kowalski, K.; Piecuch, P. The Active-Space Equation-of-Motion Coupled-Cluster Methods for Excited Electronic States: Full EOMCCSDt. *J. Chem. Phys.* **2001**, *115* (2), 643–651. https://doi.org/10.1063/1.1378323.
(101) Dutta, A. K.; Nooijen, M.; Neese, F.; Izsák, R. Exploring the Accuracy of a Low Scaling Similarity Transformed Equation of Motion Method for Vertical Excitation Energies. *J. Chem. Theory Comput.* **2018**, *14* (1), 72–91. https://doi.org/10.1021/acs.jctc.7b00802.
(102) Dutta, A. K.; Saitow, M.; Demoulin, B.; Neese, F.; Izsák, R. A Domain-Based Local Pair Natural Orbital Implementation of the Equation of Motion Coupled Cluster Method for Electron Attached States. *J. Chem. Phys.* **2019**, *150* (16), 164123. https://doi.org/10.1063/1.5089637.
(103) Nooijen, M.; Bartlett, R. J. A New Method for Excited States: Similarity Transformed Equation-of-Motion Coupled-Cluster Theory. *J. Chem. Phys.* **1997**, *106* (15), 6441–6448. https://doi.org/10.1063/1.474000.
(104) Riplinger, C.; Neese, F. An Efficient and near Linear Scaling Pair Natural Orbital Based Local Coupled Cluster Method. *J. Chem. Phys.* **2013**, *138* (3), 034106. https://doi.org/10.1063/1.4773581.
(105) Dutta, A. K.; Nooijen, M.; Neese, F.; Izsák, R. Automatic Active Space Selection for the Similarity Transformed Equations of Motion Coupled Cluster Method. *J. Chem. Phys.* **2017**, *146* (7), 074103. https://doi.org/10.1063/1.4976130.
(106) Bhattacharyya, K. Can TDDFT Render the Electronic Excited States Ordering of Azine Derivative? A Closer Investigation with DLPNO-STEOM-CCSD. *Chem. Phys. Lett.* **2021**, *779*, 138827. https://doi.org/10.1016/j.cplett.2021.138827.

(107) Berraud-Pache, R.; Neese, F.; Bistoni, G.; Izsák, R. Computational Design of Near-Infrared Fluorescent Organic Dyes Using an Accurate New Wave Function Approach. *J. Phys. Chem. Lett.* **2019**, *10* (17), 4822–4828. https://doi.org/10.1021/acs.jpclett.9b02240.
(108) Berraud-Pache, R.; Neese, F.; Bistoni, G.; Izsák, R. Unveiling the Photophysical Properties of Boron-Dipyrromethene Dyes Using a New Accurate Excited State Coupled Cluster Method. *J. Chem. Theory Comput.* **2020**, *16* (1), 564–575. https://doi.org/10.1021/acs.jctc.9b00559.
(109) Kozma, B.; Tajti, A.; Demoulin, B.; Izsák, R.; Nooijen, M.; Szalay, P. G. A New Benchmark Set for Excitation Energy of Charge Transfer States: Systematic Investigation of Coupled Cluster Type Methods. *J. Chem. Theory Comput.* **2020**, *16* (7), 4213–4225. https://doi.org/10.1021/acs.jctc.0c00154.
(110) Izsák, R. A Local Similarity Transformed Equation of Motion Approach for Calculating Excited States. *Int. J. Quantum Chem.* **2021**, *121* (3), e26327. https://doi.org/10.1002/qua.26327.
(111) Runge, E.; Gross, E. K. U. Density-Functional Theory for Time-Dependent Systems. *Phys. Rev. Lett.* **1984**, *52* (12), 997–1000. https://doi.org/10.1103/PhysRevLett.52.997.
(112) Maitra, N. T.; Burke, K. Erratum: Demonstration of Initial-State Dependence in Time-Dependent Density-Functional Theory [Phys. Rev. A 63, 042501 (2001)]. *Phys. Rev. A* **2001**, *64* (3), 039901. https://doi.org/10.1103/PhysRevA.64.039901.
(113) Maitra, N. T.; Burke, K. Demonstration of Initial-State Dependence in Time-Dependent Density-Functional Theory. *Phys. Rev. A* **2001**, *63* (4), 042501. https://doi.org/10.1103/PhysRevA.63.042501.
(114) Maitra, N. T.; Burke, K.; Woodward, C. Memory in Time-Dependent Density Functional Theory. *Phys. Rev. Lett.* **2002**, *89* (2), 023002. https://doi.org/10.1103/PhysRevLett.89.023002.
(115) Dancoff, S. M. Non-Adiabatic Meson Theory of Nuclear Forces. *Phys. Rev.* **1950**, *78* (4), 382–385. https://doi.org/10.1103/PhysRev.78.382.
(116) Tamm, Ig.; Mandelstam, L. The Uncertainty Relation Between Energy and Time in Non-Relativistic Quantum Mechanics. *J. Phys.* **1945**, No. USSR 9, 249–254.
(117) Hirata, S.; Head-Gordon, M. Time-Dependent Density Functional Theory within the Tamm–Dancoff Approximation. *Chem. Phys. Lett.* **1999**, *314* (3–4), 291–299. https://doi.org/10.1016/S0009-2614(99)01149-5.
(118) Suomivuori, C.-M.; Winter, N. O. C.; Hättig, C.; Sundholm, D.; Kaila, V. R. I. Exploring the Light-Capturing Properties of Photosynthetic Chlorophyll Clusters Using Large-Scale Correlated Calculations. *J. Chem. Theory Comput.* **2016**, *12* (6), 2644–2651. https://doi.org/10.1021/acs.jctc.6b00237.
(119) Goerigk, L. A Look at the Density Functional Theory Zoo with the Advanced GMTKN55 Database for General Main Group Thermochemistry, Kinetics and Noncovalent Interactions. **2017**.
(120) Yu, H. S.; He, X.; Truhlar, D. G. MN15-L: A New Local Exchange-Correlation Functional for Kohn–Sham Density Functional Theory with Broad Accuracy for Atoms, Molecules, and Solids. *J. Chem. Theory Comput.* **2016**, *12* (3), 1280–1293. https://doi.org/10.1021/acs.jctc.5b01082.

(121) Dohm, S.; Hansen, A.; Steinmetz, M.; Grimme, S.; Checinski, M. P. Comprehensive Thermochemical Benchmark Set of Realistic Closed-Shell Metal Organic Reactions. *J Chem Theory Comput* **2018**.
(122) Najibi, A.; Goerigk, L. The Nonlocal Kernel in van Der Waals Density Functionals as an Additive Correction: An Extensive Analysis with Special Emphasis on the B97M-V and ωB97M-V Approaches. *J. Chem. Theory Comput.* **2018**, *14* (11), 5725–5738. https://doi.org/10.1021/acs.jctc.8b00842.
(123) Morgante, P.; Peverati, R. Comparison of the Performance of Density Functional Methods for the Description of Spin States and Binding Energies of Porphyrins. **2023**.
(124) Maurer, L. R.; Bursch, M.; Grimme, S.; Hansen, A. Assessing Density Functional Theory for Chemically Relevant Open-Shell Transition Metal Reactions. *J Chem Theory Comput* **2021**.
(125) Dutta, A. K.; Neese, F.; Izsák, R. Towards a Pair Natural Orbital Coupled Cluster Method for Excited States. *J. Chem. Phys.* **2016**, *145* (3), 034102. https://doi.org/10.1063/1.4958734.
(126) Dutta, A. K.; Saitow, M.; Riplinger, C.; Neese, F.; Izsák, R. A Near-Linear Scaling Equation of Motion Coupled Cluster Method for Ionized States. *J. Chem. Phys.* **2018**, *148* (24), 244101. https://doi.org/10.1063/1.5029470.
(127) Dutta, A. K.; Saitow, M.; Demoulin, B.; Neese, F.; Izsák, R. A Domain-Based Local Pair Natural Orbital Implementation of the Equation of Motion Coupled Cluster Method for Electron Attached States. *J. Chem. Phys.* **2019**, *150* (16), 164123. https://doi.org/10.1063/1.5089637.
(128) Bouman, T. D.; Hansen, A. E.; Voigt, B.; Rettrup, S. Large-Scale RPA Calculations of Chiroptical Properties of Organic Molecules: Program RPAC. *Int. J. Quantum Chem.* **1983**, *23* (2), 595–611. https://doi.org/10.1002/qua.560230230.
(129) Bouman, T. D.; Hansen, A. E. Linear Response Calculations of Molecular Optical and Magnetic Properties Using Program RPAC: NMR Shielding Tensors of Pyridine and n-Azines. *Int. J. Quantum Chem.* **1989**, *36* (S23), 381–396. https://doi.org/10.1002/qua.560360842.
(130) Bene, J. E. D.; Ditchfield, R.; Pople, J. A. Self-Consistent Molecular Orbital Methods. X. Molecular Orbital Studies of Excited States with Minimal and Extended Basis Sets. *J. Chem. Phys.* **1971**, *55* (5), 2236–2241. https://doi.org/10.1063/1.1676398.
(131) Foresman, J. B.; Head-Gordon, M.; Pople, J. A.; Frisch, M. J. Toward a Systematic Molecular-Orbital Theory for Excited-States. *J. Phys. Chem.* **1992**, *96* (1), 135–149.
(132) Head-Gordon, M.; Rico, R. J.; Oumi, M.; Lee, T. J. A Doubles Correction to Electronic Excited States from Configuration Interaction in the Space of Single Substitutions. *Chem. Phys. Lett.* **1994**, *219* (1), 21–29. https://doi.org/10.1016/0009-2614(94)00070-0.
(133) Head-Gordon, M.; Maurice, D.; Oumi, M. A Perturbative Correction to Restricted Open Shell Configuration Interaction with Single Substitutions for Excited States of Radicals. *Chem. Phys. Lett.* **1995**, *246* (1), 114–121. https://doi.org/10.1016/0009-2614(95)01111-L.
(134) Lee, C.; Yang, W.; Parr, R. G. Development of the Colle-Salvetti Correlation-Energy Formula Into a Functional of the Electron-Density. *Phys. Rev. B* **1988**, *37*, 785–789. https://doi.org/10.1103/PhysRevB.37.785.

(135) Perdew, J. P. Density-Functional Approximation for the Correlation-Energy of the Inhomogeneous Electron-Gas. *Phys. Rev. B* **1986**, *33* (12), 8822–8824. https://doi.org/10.1103/PhysRevB.33.8822.
(136) Zhao, Y.; Truhlar, D. G. A New Local Density Functional for Main-Group Thermochemistry, Transition Metal Bonding, Thermochemical Kinetics, and Noncovalent Interactions. *J. Chem. Phys.* **2006**, *125* (19), 194101. https://doi.org/10.1063/1.2370993.
(137) Tao, J.; Perdew, J. P.; Staroverov, V. N.; Scuseria, G. E. Climbing the Density Functional Ladder: Nonempirical Meta-Generalized Gradient Approximation Designed for Molecules and Solids. *Phys. Rev. Lett.* **2003**, *91* (14), 146401. https://doi.org/10.1103/PhysRevLett.91.146401.
(138) Sun, J.; Ruzsinszky, A.; Perdew, J. P. Strongly Constrained and Appropriately Normed Semilocal Density Functional. *Phys. Rev. Lett.* **2015**, *115* (3), 036402. https://doi.org/10.1103/PhysRevLett.115.036402.
(139) Furness, J. W.; Kaplan, A. D.; Ning, J.; Perdew, J. P.; Sun, J. Accurate and Numerically Efficient r2SCAN Meta-Generalized Gradient Approximation. *J. Phys. Chem. Lett.* **2020**, *11* (19), 8208–8215. https://doi.org/10.1021/acs.jpclett.0c02405.
(140) Mardirossian, N.; Head-Gordon, M. Mapping the Genome of Meta-Generalized Gradient Approximation Density Functionals: The Search for B97M-V. *J. Chem. Phys.* **2015**, *142* (7), 074111–074132. https://doi.org/10.1063/1.4907719.
(141) Becke, A. D. Density-Functional Thermochemistry. III. The Role of Exact Exchange. *J. Chem. Phys.* **1993**, *98* (7), 5648–5652.
(142) Adamo, C.; Barone, V. Toward Reliable Density Functional Methods without Adjustable Parameters: The PBE0 Model. *J. Chem. Phys.* **1999**, *110* (13), 6158–6170. https://doi.org/10.1063/1.478522.
(143) Staroverov, V. N.; Scuseria, G. E.; Tao, J.; Perdew, J. P. Comparative Assessment of a New Nonempirical Density Functional: Molecules and Hydrogen-Bonded Complexes. *J. Chem. Phys.* **2002**, *119* (23), 12129–12137. https://doi.org/10.1063/1.1626543.
(144) Bursch, M.; Neugebauer, H.; Ehlert, S.; Grimme, S. Dispersion Corrected r2SCAN Based Global Hybrid Functionals: r2SCANh, r2SCAN0, and r2SCAN50. *J. Chem. Phys.* **2022**, *156* (13), 134105. https://doi.org/10.1063/5.0086040.
(145) Zhao, Y.; Truhlar, D. G. Design of Density Functionals That Are Broadly Accurate for Thermochemistry, Thermochemical Kinetics, and Nonbonded Interactions. *J. Phys. Chem. A* **2005**, *109* (25), 5656–5667. https://doi.org/10.1021/jp050536c.
(146) Zhao, Y.; Truhlar, D. G. The M06 Suite of Density Functionals for Main Group Thermochemistry, Thermochemical Kinetics, Noncovalent Interactions, Excited States, and Transition Elements: Two New Functionals and Systematic Testing of Four M06-Class Functionals and 12 Other Functionals. *Theor. Chem. Acc.* **2008**, *120* (1), 215–241. https://doi.org/10.1007/s00214-007-0310-x.
(147) Zhao, Y.; Truhlar, D. G. Exploring the Limit of Accuracy of the Global Hybrid Meta Density Functional for Main-Group Thermochemistry, Kinetics, and Noncovalent Interactions. *J. Chem. Theory Comput.* **2008**, *4* (11), 1849–1868. https://doi.org/10.1021/ct800246v.
(148) Yu, H. S.; He, X.; Li, S. L.; Truhlar, D. G. MN15: A Kohn–Sham Global-Hybrid Exchange–Correlation Density Functional with Broad Accuracy for Multi-Reference and

Single-Reference Systems and Noncovalent Interactions. *Chem. Sci.* **2016**, *7* (8), 5032–5051. https://doi.org/10.1039/C6SC00705H.
(149) Rohrdanz, M. A.; Herbert, J. M. Simultaneous Benchmarking of Ground- and Excited-State Properties with Long-Range-Corrected Density Functional Theory. *J. Chem. Phys.* **2008**, *129* (3), 034107. https://doi.org/10.1063/1.2954017.
(150) Rohrdanz, M. A.; Martins, K. M.; Herbert, J. M. A Long-Range-Corrected Density Functional That Performs Well for Both Ground-State Properties and Time-Dependent Density Functional Theory Excitation Energies, Including Charge-Transfer Excited States. *J. Chem. Phys.* **2009**, *130* (5), 054112–054119. https://doi.org/10.1063/1.3073302.
(151) Yanai, T.; Tew, D.; Handy, N. C. A New Hybrid Exchange-Correlation Functional Using the Coulomb-Attenuating Method (CAM-B3LYP). *Chem. Phys. Lett.* **2004**, *393* (1–3), 51–57. https://doi.org/10.1016/j.cplett.2004.06.011.
(152) Mardirossian, N.; Head-Gordon, M. *ω* B97M-V: A Combinatorially Optimized, Range-Separated Hybrid, Meta-GGA Density Functional with VV10 Nonlocal Correlation. *J. Chem. Phys.* **2016**, *144* (21), 214110. https://doi.org/10.1063/1.4952647.
(153) Peverati, R.; Truhlar, D. G. Improving the Accuracy of Hybrid Meta-GGA Density Functionals by Range Separation. *J. Phys. Chem. Lett.* **2011**, *2*, 2810–2817. https://doi.org/10.1021/jz201170d.
(154) Verma, P.; Wang, Y.; Ghosh, S.; He, X.; Truhlar, D. G. Revised M11 Exchange-Correlation Functional for Electronic Excitation Energies and Ground-State Properties. *J. Phys. Chem. A* **2019**, *123* (13), 2966–2990. https://doi.org/10.1021/acs.jpca.8b11499.
(155) Chai, J.-D.; Head-Gordon, M. Long-Range Corrected Hybrid Density Functionals with Damped Atom-Atom Dispersion Corrections. *Phys Chem Chem Phys* **2008**, *10* (44), 6615–6620. https://doi.org/10.1039/b810189b.
(156) Lin, Y.-S.; Li, G.-D.; Mao, S.-P.; Chai, J.-D. Long-Range Corrected Hybrid Density Functionals with Improved Dispersion Corrections. *J. Chem. Theory Comput.* **2012**, *9* (1), 263–272.
(157) Lin, Y.-S.; Tsai, C.-W.; Li, G.-D.; Chai, J.-D. Long-Range Corrected Hybrid Meta-Generalized-Gradient Approximations with Dispersion Corrections. *J. Chem. Phys.* **2012**, *136* (15), 154109. https://doi.org/10.1063/1.4704370.
(158) Grimme, S. Semiempirical Hybrid Density Functional with Perturbative Second-Order Correlation. *J. Chem. Phys.* **2006**, *124* (3), 034108. https://doi.org/10.1063/1.2148954.
(159) Casanova-Páez, M.; Dardis, M. B.; Goerigk, L. ωB2PLYP and ωB2GPPLYP: The First Two Double-Hybrid Density Functionals with Long-Range Correction Optimized for Excitation Energies. *J. Chem. Theory Comput.* **2019**, *15* (9), 4735–4744. https://doi.org/10.1021/acs.jctc.9b00013.
(160) Perdew, J. P.; Schmidt, K. Jacob's Ladder of Density Functional Approximations for the Exchange-Correlation Energy. *AIP Conf. Proc.* **2001**, *577* (1), 1–20. https://doi.org/10.1063/1.1390175.
(161) Loos, P.-F. Exchange Functionals Based on Finite Uniform Electron Gases. *J. Chem. Phys.* **2017**, *146* (11), 114108. https://doi.org/10.1063/1.4978409.
(162) Bannwarth, C.; Ehlert, S.; Grimme, S. GFN2-xTB—An Accurate and Broadly Parametrized Self-Consistent Tight-Binding Quantum Chemical Method with Multipole Electrostatics and Density-Dependent Dispersion Contributions. *J. Chem. Theory Comput.* **2019**, *15* (3), 1652–1671. https://doi.org/10.1021/acs.jctc.8b01176.

(163) Gordy, W.; Thomas, W. J. O. Electronegativities of the Elements. *J. Chem. Phys.* **1956**, *24* (2), 439–444. https://doi.org/10.1063/1.1742493.
(164) Neese, F.; Wennmohs, F.; Becker, U.; Riplinger, C. The ORCA Quantum Chemistry Program Package. *J. Chem. Phys.* **2020**, *152* (22), 224108. https://doi.org/10.1063/5.0004608.
(165) Lingam, M.; Loeb, A. Constraints on Aquatic Photosynthesis for Terrestrial Planets around Other Stars. *Astrophys. J.* **2020**, *889* (1), L15. https://doi.org/10.3847/2041-8213/ab6a14.
(166) Basu, M.; Mishra, P. P. Absorption Spectroscopy: What Can We Learn About Conformational Changes of Biomolecules? In *Optical Spectroscopic and Microscopic Techniques: Analysis of Biological Molecules*; Sahoo, H., Ed.; Springer Nature: Singapore, 2022; pp 1–18. https://doi.org/10.1007/978-981-16-4550-1_1.
(167) Zhu, X.-G.; Govindjee; Baker, N. R.; deSturler, E.; Ort, D. R.; Long, S. P. Chlorophyll a Fluorescence Induction Kinetics in Leaves Predicted from a Model Describing Each Discrete Step of Excitation Energy and Electron Transfer Associated with Photosystem II. *Planta* **2005**, *223* (1), 114–133. https://doi.org/10.1007/s00425-005-0064-4.
(168) Balbi, A.; Lingam, M. Beyond Mediocrity: How Common Is Life? *Mon. Not. R. Astron. Soc.* **2023**, *522* (2), 3117–3123. https://doi.org/10.1093/mnras/stad1155.

Appendix

The Appendix contains the raw data for the calculations described above, including the geometries of the molecules of interest (tables A1 – A5) and the vertical excitation energies (VEEs) in eV for the absorption bands of Chl a and the phot0 molecules (table A6, A8 - A10). Table A7 includes the data for the Tamm-Dancoff approximated (TDA) calculations and the "original" TDDFT results and provides the MUE for the TDA and TDDFT.

Table A1: Geometry (S1) of the smallest significantly representative Chl *a* molecule (xyz format), which was optimized using the CAM-B3LYP-D3(BJ)/def2-TZVP method in gas phase. Obtained from the Supporting information in Illner *et al.*[40]

76			
C	-6.94101773277842	35.79286800103698	7.98635477633448
C	-3.98102222294773	34.72352147911032	-0.68162218643282
C	2.41818178868599	37.10574470780596	3.41245195749761
C	-2.25219108797725	35.83410795974775	9.92666317325171
N	-4.55573995402007	34.85244169287340	5.83191257776971
H	-6.95620340674774	36.52504882196585	7.17750760283703
C	-4.89481255725964	34.97140548072344	-1.61150116602348
C	2.48181598256915	38.63053884709370	3.49611396655616
C	-3.73210795994643	35.42402953241709	9.54429168960854
N	-3.75420079300643	34.95221437559223	3.00064582029123
O	-1.87336348390208	35.97437278633750	11.0593395452471
C	-4.09749968731009	34.15934041884622	10.2785200864900
N	-1.85942340124899	35.79350469942186	6.43005581516318

C	-4.92442673655606	33.30847807206517	12.2946151224424
C	-3.72674232147732	35.30841136162393	8.03371472034305
C	-5.87762230053422	34.17910143776908	3.90490125603511
C	-1.94637567123760	35.53608042684566	1.47232676040621
C	0.33822428813312	36.44395180455594	5.64154956037812
C	-6.70801062326837	32.37717845011613	6.39738799170638
C	-6.58976128707013	33.75127458331651	0.91611699647059
C	0.90309353380740	36.48799076888075	0.65901366786070
C	0.92850593286370	36.72375011779826	8.76209709493966
C	-4.72304533128727	34.92584886159361	7.19675013858754
C	-5.00591773439092	34.47481367927818	2.85622278121490
C	-0.94550997379709	35.91021056990892	2.39554702753548
C	-0.55645851146418	36.20347206271686	6.67434590787102
O	-3.90057604920894	33.04441109251169	9.87900551397264
C	-6.13513701434933	34.56037242607884	7.58297763862106
C	-5.31260729403626	34.30217757237480	1.44501939468094
C	0.37992399416866	36.34352905300695	2.04797417964627
C	-0.33715210100630	36.32969602849064	8.08673771856715
O	-4.65530300455787	34.43366942549807	11.4594334667058
C	-6.66247388997242	33.90010713763338	6.30004821256342
C	-4.20805986972384	34.69978888605092	0.75626458681333

C	1.02818987790773	36.59274924832584	3.22622687259362
C	-1.54709271266898	35.98852019415750	8.66566409034399
C	-5.65579855871918	34.34437824565367	5.25983506310835
C	-3.21234644663621	35.09577835898741	1.74408156169555
C	0.08919240891217	36.31548071091521	4.28120403180639
C	-2.43004620330514	35.67266987424515	7.61435309236558
N	-1.10207774797484	35.90248175662032	3.73330560569733
Mg	-2.81936958416003	35.37504280006335	4.73082480926422
H	-6.51971340550882	36.27488130000832	8.86751455378494
H	-7.97120444011421	35.51679715844789	8.21470700459646
H	-2.96357020588187	34.52917560886468	-1.00361483443642
H	3.04461322977542	36.76349709668155	2.58723086727845
H	2.85418994697830	36.67397392994451	4.31513058727761
H	-5.91807998671285	35.21539620900278	-1.36226154263513
H	-4.63548724889499	34.96147919848033	-2.66111134393964
H	3.50762470000446	38.97339232905264	3.63593605015654
H	1.88248030415175	39.00046835447498	4.32836403859072
H	2.09254106863622	39.08456431663874	2.58446896614781
H	-4.37267789836554	36.22623887624258	9.91291470387167
H	-5.35285359181750	33.71337477307435	13.2058430354878
H	-4.00301089535288	32.77154508885973	12.5112276526719

H	-5.62426234218440	32.63084292891680	11.8087020245978
H	-6.84118958385343	33.77352009924613	3.63134868089604
H	-1.67224832888263	35.60406296471633	0.42903692747055
H	1.33111463989666	36.76910223600049	5.92329432387634
H	-7.00847192519247	31.92856356107021	5.45099676325499
H	-7.41832223918920	32.06612952140186	7.16412981773137
H	-5.72744775981967	31.98137481182714	6.66516706338777
H	-6.44267602504536	33.31291045675245	-0.06958849406966
H	-7.35614826273716	34.52438689221510	0.82150028117975
H	-6.98788109586424	32.97978677534699	1.57448868840590
H	1.95918844675213	36.75121695075061	0.66129703343982
H	0.37308342580854	37.26896561054314	0.10979316327020
H	0.79621656376052	35.56243883975556	0.09051666038683
H	1.36208053891397	37.61728465720379	8.31128588176325
H	1.67293763434527	35.92795432952511	8.69090639248266
H	0.75143746270652	36.91972204710151	9.81717960470833
H	-6.12906693109937	33.84721960099380	8.40808224216130
H	-7.65692130171338	34.27235505080080	6.04711242237590

Table A2: Geometry (S2) of the complete Chl *a* molecule (135 atoms, xyz format), which was optimized using the GFN2-xtb method. Obtained from the Supporting information in Illner *et al*.[40]

```
135

 energy: -186.255236093884 gnorm: 0.000859732492 xtb: 6.4.1 (conda-forge)

Mg       -1.16538284212160   -3.52620922994169    1.64790409848501

C        -1.72747203367702   -1.76761321193830   -1.23089086841779

C         1.66823597014874   -4.75838167490581    0.32994391849361

C        -0.69343026900199   -5.27254738249884    4.49206996217744

C        -4.04656394429298   -2.14479006977554    3.00539804209098

N        -0.19662809723576   -3.26024453352374   -0.16775000259207

C        -0.53459828725249   -2.47769116448398   -1.23316646063359

C         0.50464868809369   -2.54081589924262   -2.23989645923886

C         1.44720727211531   -3.40349524867605   -1.76318239779175

C         0.98229966155329   -3.85220937796596   -0.46634557168418

C         2.72896369261202   -3.82425815897218   -2.39309475774211

C         0.57365618479885   -1.69564539774623   -3.46509324333628

C         1.00262146723003   -0.26751054526414   -3.07937739703660

C         0.55569952357929    0.74129261705181   -4.11312785264377

O        -0.55720433453401    0.80369534086824   -4.56456536939466

O         1.55274310076092    1.56118940843654   -4.45281406870765
```

N	0.22891277564113	-4.79224490998077	2.29414966524913
C	1.31928996499788	-5.19690301226265	1.59825819692085
C	2.07761592406553	-6.14986619749014	2.37703056010406
C	1.40674419191022	-6.30128655562902	3.56342193352044
C	0.25044985757622	-5.42436218434864	3.49030017253021
C	3.36218431652437	-6.77328783540607	1.95948671886414
C	1.74657646957665	-7.12665213698784	4.70363157834626
C	2.31719057238856	-8.32440597182702	4.63931194680009
N	-2.18790091413070	-3.67038409014718	3.42416483839362
C	-1.81264887425836	-4.45080785969284	4.46233452820020
C	-2.75034708445467	-4.30921830091531	5.55772551803540
C	-3.70033417664971	-3.42623768794982	5.13907605576302
C	-3.32967395772681	-3.03142070688373	3.79455785585312
C	-2.63829832281422	-5.01244777216940	6.86538150789951
C	-4.87425662223477	-2.90058883384174	5.89600878834615
C	-4.54772359464972	-1.55237984404117	6.54348659512401
N	-2.57469049661477	-2.24313951868939	1.09697994624268
C	-3.69798904659966	-1.77315954046770	1.71361944183414
C	-4.43403074305398	-0.88665730390507	0.83521263709957
C	-3.70864456614667	-0.86802679078098	-0.33493256406632
C	-2.57435507686125	-1.71829795354830	-0.12786346089980
C	-5.69578003415131	-0.17396737949443	1.15160418829544

C	-3.65300942228294	-0.32463071575385	-1.67718010526978
O	-4.36567053543620	0.48268628881820	-2.22025254310386
C	-2.43439194934823	-1.01991459599886	-2.34886249930483
C	-2.97472827840259	-2.08385291892413	-3.29501146514508
O	-2.52268584253199	-2.35907681942995	-4.37233365150161
O	-4.01132304661814	-2.72106413661209	-2.74023909850497
C	-4.58958000479275	-3.76186444804531	-3.51401789019261
C	1.24782376008659	2.59414388852101	-5.38909383407633
C	0.48145382005251	3.71902355388093	-4.75883025489930
C	0.29017166033831	4.90428043595292	-5.32456471591100
C	0.86859614831605	5.24194901473929	-6.66831360829723
C	-0.50412731475091	5.97888893015590	-4.63988414370957
C	0.38610415152231	7.12354700212461	-4.13910424396372
C	1.37373468013415	6.64577645411978	-3.07721741727045
C	2.11294482513197	7.78306640627882	-2.36134671710124
C	2.99138624186205	8.56957236162826	-3.33143328376083
C	2.94695898429992	7.20499246978867	-1.20981594180794
C	3.44163579111084	8.26166944089888	-0.22482691603311
C	4.08371041453149	7.67301846620609	1.03373593255404
C	5.41362375007701	6.93996902071311	0.77783705793620
C	5.22680061845921	5.42450291280797	0.71773760961953
C	6.47473112884480	7.32244795251007	1.82146086827407

C	6.14917147542171	6.87395974523293	3.24612492810344
C	7.08178770231106	7.50435356210708	4.28363119395853
C	6.77823780994297	8.97347844650776	4.60391337986947
C	7.95557005773624	9.59760830367302	5.35127854610959
C	5.50636773774435	9.11244565232631	5.43768415560753
H	2.57730431684439	-5.16678034767995	-0.08797496562138
H	-0.54447070239356	-5.84963909003847	5.39351278105665
H	-4.95017093754695	-1.71992855643455	3.41763650754448
H	2.84607719095787	-3.36924324834704	-3.37269628948947
H	2.75964199393159	-4.90725258352245	-2.51098058726933
H	3.57413584471415	-3.52682265794763	-1.77220167896766
H	-0.39295983118390	-1.66397396059429	-3.96714163424154
H	1.29621466193653	-2.11132356066069	-4.16872606616872
H	2.08196297991798	-0.19938490485613	-2.94564736863400
H	0.52213469236851	0.00867124970544	-2.13618990605550
H	3.98077940380148	-6.05785078931455	1.42039784558446
H	3.18200383653617	-7.62581281428438	1.30297132153973
H	3.90988561613889	-7.12161509904052	2.83255837763350
H	1.49614251941906	-6.71096502106360	5.67234911350557
H	2.54204883273672	-8.80215579773017	3.70180493380924
H	2.55405900061371	-8.88306410349887	5.52906390016039
H	-2.60969242227618	-6.09216670398333	6.71927495069210

H	-3.48228053635902	-4.77238061253773	7.50662060155305
H	-1.72316212598440	-4.71651904528658	7.37872971256396
H	-5.15962963461987	-3.61275896954314	6.67287265982204
H	-5.72782695135396	-2.78517911798576	5.22462834048553
H	-3.72206199531607	-1.66167492473800	7.24291786170139
H	-5.41145923755952	-1.16966352133424	7.08280087410791
H	-4.25834778885899	-0.82700711184577	5.78655382162695
H	-6.00208094254414	0.42625460805515	0.29902310589007
H	-5.56120412504182	0.47759224434896	2.01529338462712
H	-6.48770323818968	-0.88487030972681	1.38826492198943
H	-1.83301863545756	-0.31553720825276	-2.92600100554937
H	-5.42342709913094	-4.14485215260154	-2.93167003910340
H	-3.85472231388739	-4.54855934961014	-3.69800836301996
H	-4.93662620713719	-3.37124393296215	-4.47261768584195
H	0.66607970313461	2.16250363951622	-6.21544103603206
H	2.21693373657634	2.92946703860355	-5.76871087435386
H	0.04998941541584	3.49415806958468	-3.79478465954370
H	0.59306420758646	4.48720118900350	-7.40323674563998
H	1.95732319953208	5.27388632419904	-6.62112021861756
H	0.51116960191050	6.20797505945417	-7.01373005179215
H	-1.04775795518093	5.55266020288102	-3.79542493923799
H	-1.23653778402546	6.38281798759584	-5.34361257269761

H	0.92430098079735	7.55507013501816	-4.98341956300923
H	-0.25174185754014	7.90168369019441	-3.71325327349207
H	2.10155942290351	5.97300872104440	-3.53558396893542
H	0.82123794987988	6.06862206424634	-2.33169707335354
H	1.36503643580538	8.46398962450708	-1.93777986864333
H	3.71091292735257	7.90793774835170	-3.80986097617300
H	3.53646304316697	9.35161319466102	-2.80970222792918
H	2.39024318747629	9.04268064869608	-4.10310009190475
H	3.79604526995120	6.66457550281316	-1.63126003257985
H	2.33304858666801	6.48704222125054	-0.66020913644676
H	2.59063155160076	8.87707134507802	0.08019664442559
H	4.16453150466074	8.91911747044809	-0.71147114359464
H	3.37390642882763	6.99475912813061	1.51158968831841
H	4.26135008348222	8.50007970506054	1.72494549776886
H	5.80035817953021	7.26953338043653	-0.19376230184324
H	4.79005105292772	5.05226868379009	1.64098198165494
H	6.18525524856110	4.93125478944869	0.56701142558433
H	4.56865422340969	5.14798507606799	-0.10115284169874
H	6.59374285634050	8.40786700765699	1.80118380333329
H	7.43362365154270	6.88716237702010	1.52727887849925
H	6.24950635266939	5.78913956891062	3.30868765889223
H	5.11507289427569	7.12233529345115	3.48395329303705

H	8.10861416698437	7.42555755218166	3.91756214354397
H	7.02163054192390	6.93244731691120	5.21296050640836
H	6.63940952322834	9.52192169994165	3.66634630440240
H	8.14057352049245	9.06148835005191	6.28008089108058
H	7.74887864196941	10.63817199985170	5.59205678499662
H	8.85979209923802	9.55943246910748	4.74758732137893
H	5.61732909556768	8.58987354540202	6.38589144852195
H	4.64606894214337	8.69917716653475	4.91752047758773
H	5.30252070741565	10.16062050275699	5.64631637113647

Table A3: Geometry of the phot0-Ca molecule (xyz format), which was optimized using the CAM-B3LYP-D3(BJ)/def2-TZVP method in gas phase. Obtained from the Supporting information in Illner *et al.*[40]

29

C	2.9892391854	1.1471639091	0.0034393674
C	2.4638805878	2.4381330409	-0.0039694790
C	1.1784519546	2.9769331795	-0.0085584206
N	2.3225414601	-0.0121581292	0.0042383118
N	0.0121715724	2.3224880802	-0.0042785723
C	-1.1471309872	2.9892354245	-0.0033572678
C	-2.4381007431	2.4639293245	0.0041500574

C	-2.9769261843	1.1784963723	0.0086679069
N	-2.3224946786	0.0122195575	0.0043313296
C	-2.9892139693	-1.1471036006	0.0031012194
C	-2.4639065337	-2.4380872921	-0.0039924460
C	-1.1784984337	-2.9769717240	-0.0082368063
N	-0.0122068398	-2.3225499012	-0.0042640142
C	1.1471368247	-2.9892192361	-0.0034051080
C	2.4381161307	-2.4638588263	0.0039778354
C	2.9769730229	-1.1784536098	0.0085804375
Ca	0.0000278399	-0.0000698166	-0.0001535426
H	4.0779258839	1.0828995018	0.0075183379
H	3.2335695403	3.2000345355	-0.0059616869
H	1.1255994786	4.0662292161	-0.0138300289
H	-1.0828199680	4.0779191222	-0.0074187649
H	-3.2000061817	3.2336140332	0.0061883761
H	-4.0662232327	1.1256598953	0.0140090715
H	-4.0779000231	-1.0828074929	0.0066925340
H	-3.2337327048	-3.1998507829	-0.0060662679
H	-1.1256935708	-4.0662715091	-0.0131424936
H	1.0828895441	-4.0779072086	-0.0073630619
H	3.1998955002	-3.2336694883	0.0060703889
H	4.0662689040	-1.1256331621	0.0140360110

Table A4: Geometry (S4) of the phot0-Mg molecule (xyz format), which was optimized using the CAM-B3LYP-D3(BJ)/def2-TZVP method in gas phase. Obtained from the Supporting information in Illner *et al*.[40]

```
29

C       1.3689887787    -2.7790501944    -0.0000000000

C       0.1543492219    -3.4222136696     0.0000000000

C      -1.1132294773    -2.8910067338     0.0000000000

N       1.5922523169    -1.4546031633    -0.0000000000

N      -1.4545681959    -1.5921736076    -0.0000000000

C      -2.7790183151    -1.3689094887    -0.0000000000

C      -3.4222043245    -0.1542819408    -0.0000000000

C      -2.8910235135     1.1133080687    -0.0000000000

N      -1.5921961557     1.4546588145    -0.0000000000

C      -1.3689312073     2.7791053598    -0.0000000000

C      -0.1542936558     3.4222745409     0.0000000000

C       1.1132878784     2.8910706284     0.0000000000

N       1.4546301085     1.5922401790    -0.0000000000

C       2.7790796708     1.3689741471    -0.0000000000

C       3.4222600660     0.1543436440    -0.0000000000

C       2.8910775150    -1.1132472011    -0.0000000000

Mg      0.0000288916     0.0000060092    -0.0000000000

H       2.2527652200    -3.4128227569     0.0000000000
```

H	0.2028120807	-4.5028261269	0.0000000000
H	-1.9366164862	-3.6014601610	0.0000000000
H	-3.4127849601	-2.2526901033	-0.0000000000
H	-4.5028155388	-0.2027712393	0.0000000000
H	-3.6014901216	1.9366847258	0.0000000000
H	-2.2527070310	3.4128801907	-0.0000000000
H	-0.2027619164	4.5028873142	0.0000000000
H	1.9366720074	3.6015290174	0.0000000000
H	3.4128508111	2.2527524639	0.0000000000
H	4.5028720094	0.2028271116	-0.0000000000
H	3.6015469516	-1.9366217292	-0.0000000000

Table A5: Geometry (S5) phot0-Ca molecule (xyz format), which was optimized using the CAM-B3LYP-D3(BJ)/def2-TZVP method in gas phase. Obtained from the Supporting information in Illner *et al*.[40]

29

C	-1.6758236900	-2.5900315753	-0.0128403480
C	-2.8534355177	-1.8881045675	-0.0036397532
C	-3.0408011703	-0.5301473973	0.0022005989
N	-0.4279085833	-2.0950663138	-0.0135152410
N	-2.0985791303	0.4261313548	-0.0025364209
C	-2.5934764191	1.6739962782	-0.0029149319
C	-1.8916345680	2.8515611934	-0.0125767263

C	-0.5336833615	3.0389883937	-0.0187279729
N	0.4225862473	2.0968359543	-0.0136679199
C	1.6705293845	2.5918616972	-0.0121459653
C	2.8481617450	1.8900020483	-0.0033911578
C	3.0355801777	0.5319451537	0.0019916388
N	2.0932300764	-0.4243456774	-0.0023616597
C	2.5883474994	-1.6723540147	-0.0025842168
C	1.8864521254	-2.8500491291	-0.0120451513
C	0.5283980201	-3.0374461632	-0.0184697843
Zn	-0.0028526776	0.0010467845	-0.0077544672
H	-1.7546913347	-3.6741123238	-0.0180097634
H	-3.7548130113	-2.4856532124	-0.0013921247
H	-4.0702412088	-0.1811624795	0.0083601292
H	-3.6774447541	1.7528563203	0.0028937675
H	-2.4891254108	3.7529227486	-0.0147183217
H	-0.1847046532	4.0684423686	-0.0253096347
H	1.7493946023	3.6759035960	-0.0164511014
H	3.7496318255	2.4874993177	-0.0010847786
H	4.0651479737	0.1828729863	0.0076692170
H	3.6725010435	-1.7511845357	0.0030350451
H	2.4840548017	-3.7515038392	-0.0140861413
H	0.1793697294	-4.0670019633	-0.0252220694

Table A6: Vertical Excitation Energies (in eV) calculated for the Q- and B-bands of Chlorophyll *a* with the DLPNO-STEOM-CCSD method and compared to various TD-DFT exchange–correlation functionals with geometry S2. Obtained from the Supporting information in Illner *et al.*[40]

Method:	**Q_y**	**State #**	**Q_x**	**State #**	**B_x**	**State #**	**B_y**	**State #**
Exp	**1.99**	**1**	**2.3**	**2**	**3.12**	**3**	**3.38**	**4**
DLPNO	**1.75**	**1**	**2.24**	**2**	**3.17**	**3**	**3.40**	**4**
BLYP	2.06	1	2.09	2	3.06	11	3.19	16
PBE	2.07	1	2.10	2	2.90	11	3.10	15
BP86	2.07	1	2.10	2	2.84	12	3.08	15
M06-L	2.16	1	2.17	2	3.02	11	3.30	14
MN15-L	2.29	1	2.31	2	3.10	11	3.22	14
TPSS	2.11	1	2.14	2	2.94	11	3.16	15
SCAN	2.16	1	2.17	2	3.00	11	3.11	15
B97M-V	2.19	1	2.21	2	2.99	11	3.12	15
B3LYP	2.22	1	2.26	2	3.13	3	3.21	4
PBE0	2.25	1	2.29	2	3.15	3	3.23	4
TPSSh	2.21	1	2.22	2	3.10	3	3.18	4
r2SCANh	2.26	1	2.28	2	3.20	3	3.29	4
r2SCAN0	2.30	1	2.35	2	3.25	3	3.33	4
PW6B95	2.24	1	2.28	2	3.15	3	3.23	4
M06	2.16	1	2.21	2	3.12	3	3.20	4

M06-2X	2.25	1	2.32	2	3.36	3	3.41	4
M08-HX	2.28	1	2.35	2	3.36	3	3.41	4
MN15	2.22	1	2.28	2	3.25	3	3.31	4
CAM-B3LYP	2.17	1	2.24	2	3.35	3	3.40	4
ωB97M-V	2.02	1	2.09	2	3.40	3	3.43	4
ωB97X-V	2.01	1	2.09	2	3.45	3	3.48	4
M11	2.08	1	2.16	2	3.42	3	3.45	4
revM11	1.91	1	2.00	2	3.42	3	3.43	4

Table A7: Comparison between the Vertical Excitation Energies (VEEs, in eV) for the Q- and B-bands of Chl a, calculated with the "regular" TD-DFT and TD-DFT approximated with the Tamm–Dancoff approximation (TDA) with various exchange–correlation functionals with geometry S2. The last two columns report the mean unsigned errors (MUE) of both methods. Obtained from the Supporting information in Illner *et al.*[40]

	Q_y		Q_x		B_x		B_y			
Exp	**1.99**		**2.30**		**3.12**		**3.38**			
	TDDFT	**TDA**	**TDDFT**	**TDA**	**TDDFT**	**TDA**	**TDDFT**	**TDA**	**MUE TDDFT**	**MUE TDA**
CIS/RPA	2.45	2.05	3.48	3.22	4.29	3.89	4.84	4.52	1.07	0.72
BLYP	2.05	2.13	2.13	2.14	2.82	2.86	2.95	2.96	0.24	0.25
PBE	2.07	2.13	2.14	2.15	2.83	2.85	2.96	2.98	0.24	0.24
BP86	2.06	2.15	2.14	2.36	2.84	3.01	2.96	3.11	0.23	0.15
M06-L	2.13	2.27	2.24	2.33	3.01	3.18	3.15	3.27	0.14	0.12
MN15-L	2.23	2.38	2.38	2.45	3.17	3.36	3.34	3.57	0.10	0.24
r2SCAN	2.16	2.25	2.26	2.26	3.01	3.06	3.15	3.21	0.14	0.13
B97M-V	2.15	2.25	2.28	2.26	3.05	3.12	3.20	3.25	0.11	0.11
B3LYP	2.16	2.31	2.35	2.43	3.17	3.13	3.35	3.42	0.07	0.13
r2SCANh	2.20	2.32	2.35	2.33	3.17	3.32	3.33	3.38	0.09	0.14
r2SCAN0	2.24	2.38	2.47	2.41	3.36	3.43	3.56	3.64	0.21	0.27
PW6B95	2.17	2.31	2.40	2.35	3.22	3.30	3.27	3.35	0.12	0.15
M06	2.11	2.25	2.35	2.28	3.23	3.33	3.42	3.51	0.08	0.16

M06-2X	2.19	2.39	2.56	2.45	3.44	3.77	3.69	3.87	0.27	0.42
M08-HX	2.21	2.4	2.56	2.68	3.44	3.69	3.68	3.8	0.27	0.45
M08-SO	2.15	2.34	2.54	2.66	3.41	3.71	3.68	3.8	0.25	0.43
MN15	2.15	2.33	2.47	2.38	3.33	3.58	3.56	3.71	0.18	0.30
LC-ωPBE	2.07	2.26	2.59	2.29	3.47	3.37	3.78	3.45	0.28	0.15
CAM-B3LYP	2.14	2.33	2.53	2.39	3.43	3.76	3.71	3.85	0.26	0.39

Table A8: Vertical Excitation Energies (in eV) of the Q- and B-bands for the phot0-Ca molecule, calculated with the DLPNO-STEOM-CCSD method and compared to various TD-DFT exchange–correlation functionals with the geometry in S3. Obtained from the Supporting information in Illner *et al.*[40]

	Q_y	Q_x	B_y	B_x
DLPNO-STEOM-CCSD	2.141	2.141	3.77	3.775
B2PLYP	2.219	2.219	3.421	3.421
ωB2PLYP	1.971	1.971	3.615	3.615
PW6B95	2.195	2.195	3.513	3.513
M06	2.116	2.116	3.468	3.468
B3LYP	2.174	2.174	3.448	3.448
MN15	2.135	2.135	3.538	3.538
M08-SO	2.099	2.099	3.557	3.447
CAM-B3LYP	2.069	2.069	3.592	3.592
PBE0	2.219	2.219	3.547	3.547
LC-ωPBEh	2.067	2.067	3.626	3.626
ωB97X-D	2.043	2.043	3.623	3.623
LC-ωPBE	1.968	1.968	3.635	3.635
TPSSh	2.213	2.213	3.477	3.477
M06-2X	2.165	2.165	3.616	3.616

M08-HX	2.216	2.216	3.575	3.624
ωM05-D	2.053	2.053	3.647	3.647
B97M-V	2.180	2.180	3.458	3.458
r^{2}SCANh	2.258	2.258	3.567	3.567
r^{2}SCAN0	2.263	2.263	3.664	3.664
ωB97X-D3	1.969	1.969	3.659	3.659
ωB97M-V	1.894	1.894	3.597	3.597
ωM06-D3	1.940	1.940	3.670	3.670
SCAN	2.110	2.110	3.501	3.501
MN15-L	2.273	2.273	3.608	3.608
M06-L	2.222	2.222	3.510	3.510
r^{2}SCAN	2.230	2.230	3.492	3.492
revM11	1.796	1.796	3.660	3.660
ωB97X-V	1.895	1.895	3.679	3.679
TPSS	2.112	2.112	3.531	3.531
M11	2.006	2.006	3.681	3.681
BP86	2.129	2.129	3.284	3.284
PBE	2.133	2.133	3.287	3.287
BLYP	2.093	2.093	3.229	3.229

Table A9: Vertical Excitation Energies (in eV) of the Q- and B-bands for the phot0-Mg molecule, calculated with the DLPNO-STEOM-CCSD method and compared to various TD-DFT exchange–correlation functionals with the geometry in S4. Obtained from the Supporting information in Illner *et al.*[40]

	Q_y	Q_x	B_y	B_x
DLPNO-STEOM-CCSD	2.165	2.166	3.900	3.900
B2PLYP	2.219	2.219	3.678	3.678
ωB2PLYP	1.978	1.978	3.894	3.894
PW6B95	2.216	2.216	3.835	3.835
M06	2.136	2.136	3.779	3.779
B3LYP	2.209	2.209	3.791	3.791
MN15	2.139	2.139	3.851	3.851
M08-SO	2.103	2.103	3.882	3.882
CAM-B3LYP	2.089	2.089	3.931	3.931
PBE0	2.237	2.237	3.860	3.860
LC-ωPBEh	2.087	2.087	3.945	3.945
ωB97X-D	2.062	2.062	3.944	3.944
LC-ωPBE	2.087	2.087	3.945	3.945
TPSSh	2.245	2.245	3.791	3.791
M06-2X	2.174	2.174	3.940	3.940
M08-HX	2.224	2.224	3.936	3.936

ωM05-D	2.058	2.058	3.944	3.944
B97M-V	2.233	2.233	3.822	3.822
r^{2}SCANh	2.283	2.283	3.881	3.881
r^{2}SCAN0	2.271	2.271	3.970	3.970
ωB97X-D3	1.987	1.987	3.976	3.976
ωB97M-V	1.922	1.922	3.940	3.940
ωM06-D3	1.957	1.957	3.992	3.992
SCAN	2.143	2.143	3.828	3.828
MN15-L	2.304	2.304	3.949	3.949
M06-L	2.252	2.252	3.794	3.794
r^{2}SCAN	2.270	2.270	3.816	3.816
revM11	1.823	1.823	3.966	3.966
ωB97X-V	1.918	1.918	4.002	4.002
TPSS	2.171	2.171	3.653	3.653
M11	2.012	2.012	3.976	3.976
BP86	2.187	2.187	3.635	3.635
PBE	2.193	2.193	3.638	3.638
BLYP	2.164	2.164	3.609	3.609

Table A10: Vertical Excitation Energies (in eV) of the Q- and B-bands for the phot0-Mg molecule, calculated with the DLPNO-STEOM-CCSD method and compared to various TD-DFT exchange–correlation functionals with the geometry in S5. Obtained from the Supporting information in Illner *et al.*[40]

	Q_y	Q_x	B_y	B_x
DLPNO-STEOM-CCSD	2.210	2.214	3.985	3.986
B2PLYP	2.267	2.267	3.746	3.746
ωB2PLYP	2.038	2.038	3.974	3.974
PW6B95	2.262	2.262	3.904	3.904
M06	2.186	2.186	3.844	3.844
B3LYP	2.256	2.256	3.855	3.855
MN15	2.188	2.188	3.932	3.932
M08-SO	2.154	2.154	3.965	3.965
CAM-B3LYP	2.141	2.141	4.009	4.009
PBE0	2.281	2.281	3.927	3.927
LC-ωPBEh	2.138	2.138	4.022	4.022
ωB97X-D	2.116	2.116	4.022	4.022
LC-ωPBE	2.047	2.047	4.023	4.023
TPSSh	2.290	2.290	3.851	3.851
M06-2X	2.227	2.227	4.030	4.030
M08-HX	2.276	2.276	4.022	4.022

ωM05-D	2.111	2.111	4.032	4.032
B97M-V	2.281	2.281	3.878	3.878
r^{2}SCANh	2.328	2.328	3.943	3.943
r^{2}SCAN0	2.316	2.316	4.040	4.040
ωB97X-D3	2.044	2.044	4.057	4.057
ωB97M-V	1.981	1.982	4.029	4.029
ωM06-D3	2.017	2.017	4.085	4.085
SCAN	2.195	2.195	3.888	3.888
MN15-L	2.358	2.358	4.025	4.025
M06-L	2.307	2.307	3.861	3.861
r^{2}SCAN	2.316	2.316	3.870	3.870
revM11	1.885	1.885	4.049	4.049
ωB97X-V	1.977	1.977	4.088	4.088
TPSS	2.223	2.223	3.709	3.710
M11	2.066	2.066	4.057	4.057
BP86	2.233	2.233	3.684	3.684
PBE	2.239	2.239	3.687	3.687
BLYP	2.211	2.211	3.656	3.656